

# Engineering a Novel Probiotic Toolkit in *Escherichia coli* Nissle 1917 for Sensing and Mitigating Gut Inflammatory Diseases

Nathalie Weibel,<sup>▽</sup> Martina Curcio,<sup>▽</sup> Atilla Schreiber,<sup>▽</sup> Gabriel Arriaga,<sup>▽</sup> Marine Mausy,<sup>▽</sup> Jana Mehdy, Lea Brüllmann, Andreas Meyer, Len Roth, Tamara Flury, Valerie Pecina, Kim Starlinger, Jan Dergič, Kenny Jungfer, Fabian Ackle, Jennifer Earp, Martin Hausmann, Martin Jinek, Gerhard Rogler, and Cauã Antunes Westmann\*



Cite This: *ACS Synth. Biol.* 2024, 13, 2376–2390



Read Online

ACCESS |



Metrics & More

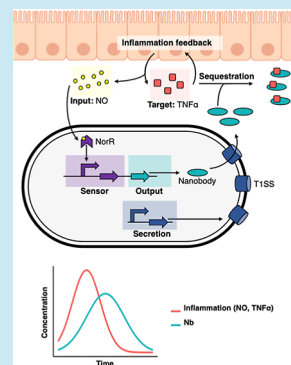


Article Recommendations



Supporting Information

**ABSTRACT:** Inflammatory bowel disease (IBD) is characterized by chronic intestinal inflammation with no cure and limited treatment options that often have systemic side effects. In this study, we developed a target-specific system to potentially treat IBD by engineering the probiotic bacterium *Escherichia coli* Nissle 1917 (EcN). Our modular system comprises three components: a transcription factor-based sensor (NorR) capable of detecting the inflammation biomarker nitric oxide (NO), a type 1 hemolysin secretion system, and a therapeutic cargo consisting of a library of humanized anti-TNF $\alpha$  nanobodies. Despite a reduction in sensitivity, our system demonstrated a concentration-dependent response to NO, successfully secreting functional nanobodies with binding affinities comparable to the commonly used drug Adalimumab, as confirmed by enzyme-linked immunosorbent assay and in vitro assays. This newly validated nanobody library expands EcN therapeutic capabilities. The adopted secretion system, also characterized for the first time in EcN, can be further adapted as a platform for screening and purifying proteins of interest. Additionally, we provided a mathematical framework to assess critical parameters in engineering probiotic systems, including the production and diffusion of relevant molecules, bacterial colonization rates, and particle interactions. This integrated approach expands the synthetic biology toolbox for EcN-based therapies, providing novel parts, circuits, and a model for tunable responses at inflammatory hotspots.



**KEYWORDS:** *engineered probiotic, IBD, inflammation, E. coli* Nissle 1917 (EcN), nitric oxide, TNF $\alpha$ , nanobodies

## INTRODUCTION

Inflammatory bowel diseases (IBD) are chronic relapsing inflammations of the gastrointestinal tract that affect more than six million people worldwide.<sup>1–5</sup> Inflammation of the intestinal mucosa compromises barrier function, exposing deeper gastrointestinal layers to luminal antigens and microbiota, which triggers aberrant immune responses and maintains local and systemic inflammation.<sup>2</sup> Current pharmacological interventions aim to induce clinical remission by reducing mucosal inflammation and alleviating disease symptoms.

Among the approved therapies for IBD,<sup>6</sup> monoclonal antibodies against pro-inflammatory cytokines like tumor necrosis factor (TNF $\alpha$ ), IL-12/23, or integrins are particularly effective.<sup>6</sup> TNF $\alpha$  is a key pro-inflammatory mediator with elevated levels in inflamed gut tissue,<sup>7</sup> making it an attractive drug target with demonstrated therapeutic benefit.<sup>6,8,9</sup> However, the systemic action of these therapeutics can lead to immunosuppression, increasing the risk of serious infections and lymphoma.<sup>8,10</sup> Therefore, there is a high demand for new therapeutic solutions that target mucosal inflammation more precisely and are cost-effective.<sup>3,10,11</sup>

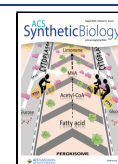
Engineered probiotics<sup>12,13</sup> offer a potential solution for such treatments, being able to reach inflammatory hotspots in the gut where the mucus barrier is compromised by chronic inflammation.<sup>14</sup> The probiotic *Escherichia coli* Nissle 1917 (EcN)<sup>15–17</sup> is naturally present in the human gut and has been widely used to treat intestinal diseases due to its anti-inflammatory and antimicrobial properties.<sup>17–24</sup> Thus, EcN is a promising chassis for targeted gut therapies.<sup>25</sup> Over the past decade, this strain has been extensively engineered to produce biomolecules at disease sites, particularly for treating intestinal diseases.<sup>26–33</sup> However, despite recent developments in expanding the tools and biological parts for engineering EcN, there remains a shortage of self-regulating genetic circuits that can recognize specific biomarkers and respond by producing therapeutic molecules.<sup>34</sup>

**Received:** January 18, 2024

**Revised:** June 13, 2024

**Accepted:** July 25, 2024

**Published:** August 8, 2024



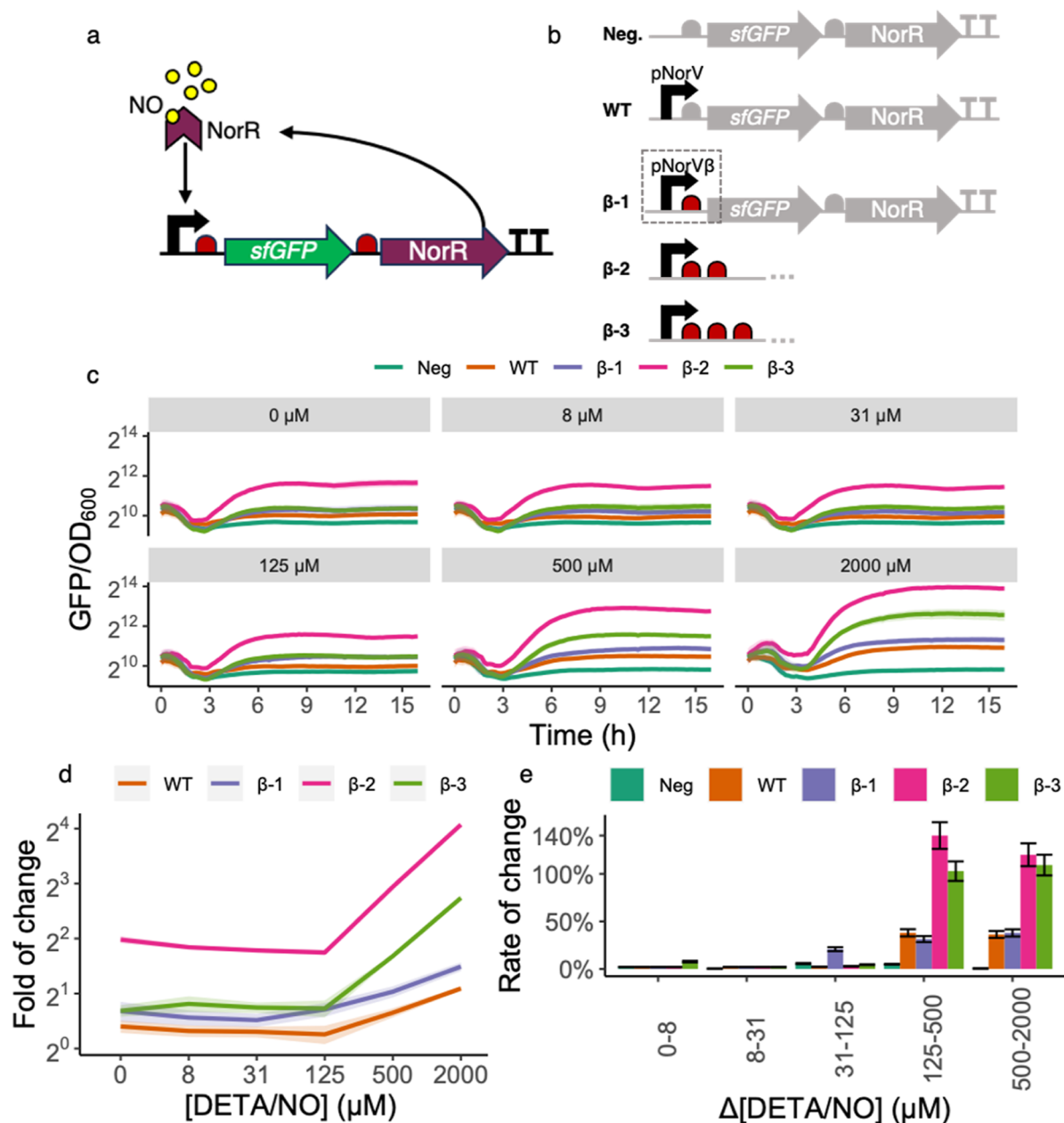


**Figure 1.** Design and characterization of the NO detection module. (a) NO-dependent activation from NorR. The NorR transcription factor (represented by the purple chevron) binds its cognate binding site at the promoter pNorV $\beta$  (black arrow). When not bound to NO (yellow circles), NorR acts as a competitive inhibitor of its NO-bound form and represses pNorV $\beta$ . However, at high NO concentrations, the NO-bound form of NorR is predominant and acts as a positive inducer of pNorV $\beta$ . The presence of *norR* in the inducible operon generates a positive feedback mechanism. Ribosomes are represented in red and the *sfGFP* gene in green. (b) Construct variants characterized. Our original construct  $\beta$ -1 consisted of *sfGFP* and *norR*, preceded by one RBS each, and placed under the control of the optimized promoter pNorV $\beta$ . To avoid read-through, we placed a double-terminator at the end of the operon. We normalized the responses of  $\beta$ -1,  $\beta$ -2, and  $\beta$ -3 to a negative control (Neg) and compared to a positive control (WT). Neg consisted of *sfGFP* and *norR* genes, preceded by one RBS each, and did not contain any promoter, accounting for the intrinsic leakiness of our module. WT consisted of *sfGFP* and *norR* genes, preceded by one RBS each, and placed under the control of the wild-type promoter pNorV. (c) Time-lapse fluorescence assay for construct characterization. We have grown each construct for 16 h (*x*-axis) on a microplate reader where green fluorescence (arbitrary units) and measured the culture's OD<sub>600</sub> every 15 min. The *y*-axis represents normalized fluorescence values (*sfGFP*/OD<sub>600</sub>). Each panel grid represents a different concentration of DETA/NO used to test individual constructs. The DETA/NO gradients we used were 0, 8, 31, 125, 500, and 2000  $\mu$ M. Each line color represents a construct. Line shadings represent the standard deviation of our biological replicates (*n* = 3). We performed all measurements with both biological and technical triplicates. Notice that measurements are on log<sub>2</sub> scale to facilitate data visualization. (d) Fold of change for each construct. Each curve represents the fold of change for each construct at *T* = 8 h along a gradient of NO concentrations. Line shadings represent the standard deviation of our biological replicates (*n* = 3). Notice that measurements are on the log<sub>2</sub> scale to facilitate data visualization. (e) Rate of change for each construct. The bar plots represent the rate of change for each construct for each DETA/NO change of concentration at *T* = 8 h. We calculated rates of change as the relative increase in fluorescence (reported as percentages, *y*-axis) from an initial NO concentration to the next incremental one. We have performed such calculations for each consecutive pair of concentrations (*x*-axis). Error bars represent the standard deviation of our biological replicates (*n* = 3).

To address this challenge and contribute to the expansion of the EcN synthetic biology toolbox, we designed, engineered, and characterized a new genetic circuit for EcN to act as a biotherapeutic against gut inflammation. This circuit detects NO as a biomarker and responds by producing and secreting nanobodies to sequester TNF $\alpha$  and locally reduce inflammation. To date, only one other study has created a similar functional system, however, without a biomarker-induced expression and using alternative components in their circuitry.<sup>33</sup> The scarcity of such systems in EcN highlights the need for alternative systems such as the one presented in our study.

NO is a free radical synthesized by inducible NO synthase in gut epithelial cells, with increased concentrations at inflamed sites.<sup>35,36</sup> This small molecule can also penetrate bacterial membranes without specialized surface receptors,<sup>37</sup> making it an effective biomarker for inflammation. In this study, we utilized a NO biosensor endogenous to *E. coli*, specifically the NorR-pNorV system, which was previously modified and characterized by Chen et al.,<sup>38</sup> to trigger the expression of the nanobody delivery system.

Nanobodies, single-domain antibodies that can bind specific antigens,<sup>39,40</sup> are advantageous in therapeutic applications due to their superior tissue penetration, stability, and ease of production by bacteria.<sup>33</sup> These nanobodies can be “humanized” to reduce immunogenicity by modifying specific amino acids.<sup>41</sup> In this study, we used humanized nanobodies developed by Silence et al.,<sup>42</sup> producing them for the first time in EcN.

The secretion of nanobodies is essential for TNF $\alpha$  inactivation since this cytokine is present in the gut extracellular environment. Most secretion systems in Gram-negative bacteria such as EcN typically release proteins into the periplasmic space rather than the surrounding environment.<sup>43</sup> Thus, we utilized the Type I hemolysin A secretion system from uropathogenic *E. coli*.<sup>44–48</sup> This system has the advantage of being one of the smallest secretion complexes in Gram-negative bacteria, and its functionality has not been described in EcN before.

Thus, in this study, we engineered a novel self-regulated system to produce and secrete anti-TNF $\alpha$  nanobodies in response to NO, aiming to reduce intestinal inflammation. Our data shows that although NO sensitivity was lower than reported in a previous study,<sup>38</sup> our system successfully expressed a variety of humanized nanobodies in an inducible manner. We also demonstrate that the produced nanobodies can be effectively secreted to the extracellular environment, retaining their functional capabilities to bind TNF $\alpha$  and reduce inflammation in cell-based assays. This indicates that this system can also facilitate the screening and purification of nanobodies or other proteins of interest in future studies using EcN. Lastly, we developed a mathematical framework to investigate relevant parameters for gut inflammation treatment, addressing the scarcity of modeling tools for such systems.

## RESULTS

**Experimental Design.** We designed our system by integrating two independent modules on separate plasmids: a sensing module and a secretion module. The sensing module recognizes NO concentrations through the NorR transcription regulator and promotes the production of nanobodies in an inducible manner. The secretion module encodes a secretion system that allows the secretion of nanobodies into the

extracellular environment. We characterized each component of our system independently before combining the complete engineered device. This allowed us not only to provide a proof of concept for each subsystem but also to optimize some of them in an iterative process. First, we assessed different architectures of our sensing system through fluorescence reporter-based assays, characterizing their limit of detection and output fold-change in response to different NO concentrations. Second, we assessed the production and secretion of nanobodies and their activity using *in vitro* and cell-based assays. Finally, we tested the whole device and its ability to produce nanobodies in an induced manner. We complemented our study with a simple yet insightful mathematical framework assessing the interactions between the EcN and inflammation sites. This framework focuses on the production rates of NO and TNF $\alpha$ , as well as the bacterial response to NO through the production of anti-TNF $\alpha$  nanobodies.

**Characterization of the NO Sensing Module.** To create an inducible system that can sense and respond to inflammation in the gut, we chose a NO-sensitive genetic circuit based on the NorR regulator. NorR is an endogenous transcription factor from *E. coli* responsible for sensing NO concentrations and modulating the expression of genes that are essential for NO detoxification under anaerobic conditions.<sup>49,50</sup> NorR interacts with NO through a non-haem iron center and binds cooperatively to three enhancer sites at the pNorV promoter to regulate transcription of both *norVW* genes and its own divergently transcribed gene (*norR*).<sup>49–51</sup> In *E. coli*, it thereby regulates the activity of the target *norV* gene in a NO-dependent manner. At low NO concentrations, NorR is predominantly present in its free form, which inhibits pNorV. However, at higher concentrations of NO, the radical binds NorR, inducing a conformational change of this protein, which makes it now able to promote  $\sigma$ 54-dependent translational activation.<sup>52</sup>

We based the design of our sensor on a previous study by Chen et al.,<sup>38</sup> consisting of the promoter pNorV $\beta$ , an optimized variant of the natural *E. coli* K-12 pNorV lacking the second integration host factor binding site.<sup>38</sup> We placed the promoter upstream a bicistronic operon containing genes encoding for a superfolder GFP (*sfGFP*)<sup>53</sup> and for the NorR regulator (*norR*), in this order. The regulatory logic relies on a positive feedback loop that modulates NorR availability in a NO-dependent manner<sup>38</sup> (Figure 1a, see Supporting Information Methods and Figures S1–S3 for more information about constructs and plasmids). This architecture ensures low inhibitory NorR levels in the cells but high availability of activated NorR in environments with a high NO concentration.<sup>38</sup> Due to the potential cellular toxicity of NO,<sup>54</sup> we verified that the concentrations used did not influence EcN cell growth in our experiments (Figure S4). Removal of the positive feedback loop decreases the induced expression of downstream genes (see Figure S5). To characterize and compare our NO-sensing constructs' limit of detection and dynamic range, we performed time-lapse fluorescence plate reader assays. We performed these experiments using EcN cells.

We observed that the NorR circuit design with the best performance in the original study<sup>38</sup> featured three consecutive ribosome binding sites (RBSs) upstream of the *sfGFP* gene. To investigate the impact of altering the number of consecutive RBSs on the sensitivity of our system, we designed,

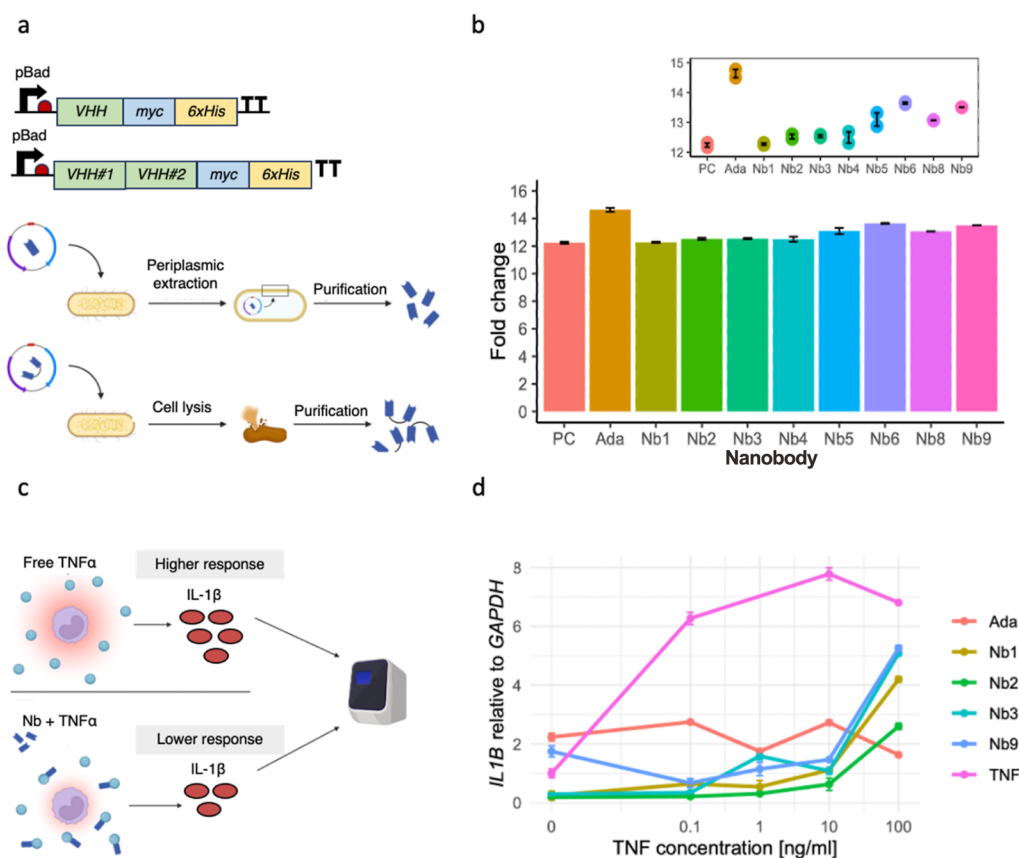


**Figure 2.** Design and characterization of the purified anti-TNF $\alpha$  nanobodies. (a) Design of monovalent and bivalent anti-TNF $\alpha$  nanobodies. We linked bivalent nanobody constructs via a short peptide linker (EPKTPKPQAAAA). To characterize the nanobodies, we added a myc-tag and a his-tag to their C-terminal sites. Their expression was under the control of the inducible pBad system, which relies on the addition of *L*-arabinose. We induced the expression of nanobodies with the pBad inducible system. We harvested monovalent nanobodies via periplasmic extraction and bivalent nanobodies through whole-cell lysis. We purified all nanobodies by immobilized metal anion chromatography. (b) Testing binding capability of purified nanobodies with ELISA. We tested TNF $\alpha$ -binding using an ELISA by capturing the purified nanobodies via their myc-tag. Then, we visualized the binding of nanobodies to biotinylated TNF $\alpha$  with the streptavidin-peroxidase. We measured the absorbance of each well with a plate reader and analyzed the fold change with R studio. (c) Overview of the cell assay used to determine anti-inflammatory properties of purified anti-TNF $\alpha$  nanobodies. We incubated Human THP-1 monocytes with rTNF $\alpha$  and different purified anti-TNF $\alpha$  nanobodies. We assessed the immune response of the monocytic cell line to rTNF $\alpha$  by quantitatively determining the *IL1B* expression levels with the use of RT-qPCR. The binding of the nanobodies to rTNF $\alpha$  is supposed to inhibit the inflammatory effect observed in untreated but stimulated THP-1 cells. (d) *IL1B* expression compared to *GAPDH* in human THP-1 monocytic cell line. Quantitative analysis of the inflammatory *IL1B* expression levels revealed a decreased immune response of rTNF $\alpha$ -stimulated cells when purified nanobodies were added, compared to untreated cells (labeled as “TNF”, pink line). Adalimumab is an anti-TNF $\alpha$  monoclonal antibody frequently used in the clinic to treat IBD patients and served in this experiment as a positive control.

constructed, and characterized three variants with one, two, or three consecutive RBSs, respectively named  $\beta$ -1,  $\beta$ -2, and  $\beta$ -3 (Figure 1b). This approach allowed us to assess the effect of varying the number of RBSs on the sensitivity of our system. To account for background fluorescence, we systematically compared our constructs to a negative control plasmid that did not contain any promoter (Figure 1b). We also compared our constructs to the wild-type pNorV with a single RBS (Figure 1b).

**Number of RBSs Upstream of *sfGFP* Influences Its Expression Levels and the Leakiness of the Construct.** Our first observation was that the pNorV $\beta$  system exhibited higher fluorescence levels than the wild-type, regardless of the NO concentration (Figure 1c), indicating this system is leakier than the wild-type. By changing the number of RBSs, we observed differences in our detection limits and the overall fluorescent reporter expression. We can observe in Figure 1c that our constructs can be increasingly ranked regarding basal

*sfGFP* expression as  $WT < \beta$ -1 <  $\beta$ -3 <  $\beta$ -2. Interestingly, the consecutive addition of RBSs does not result in a linear increase in *sfGFP* expression. We speculate that this phenomenon may be due to structural consequences arising from repeating sequences in tandem, such as the potential formation of secondary structures or hairpins.<sup>55</sup> Additionally, ribosome stalling could occur, where ribosomes pause or slow down due to interactions between ribosomes initiated at different RBSs.<sup>56,57</sup>

We observed that  $\beta$ -2 is highly leaky, showing higher *sfGFP* expression even in the absence of induction ( $[NO] = 0$ ). The higher expression baseline of  $\beta$ -2 *sfGFP* expression can also be highlighted in Figure 1d, showing the fold-of change in *sfGFP* expression for each construct at all tested NO concentrations. We also observed in Figure 1d that  $\beta$ -1 responds to a lower concentration than the other constructs ( $[NO] = 125 \mu M$ ). This is further illustrated in Figure 1e, which shows the rate of change, a sensitivity metric for each genetic construct to

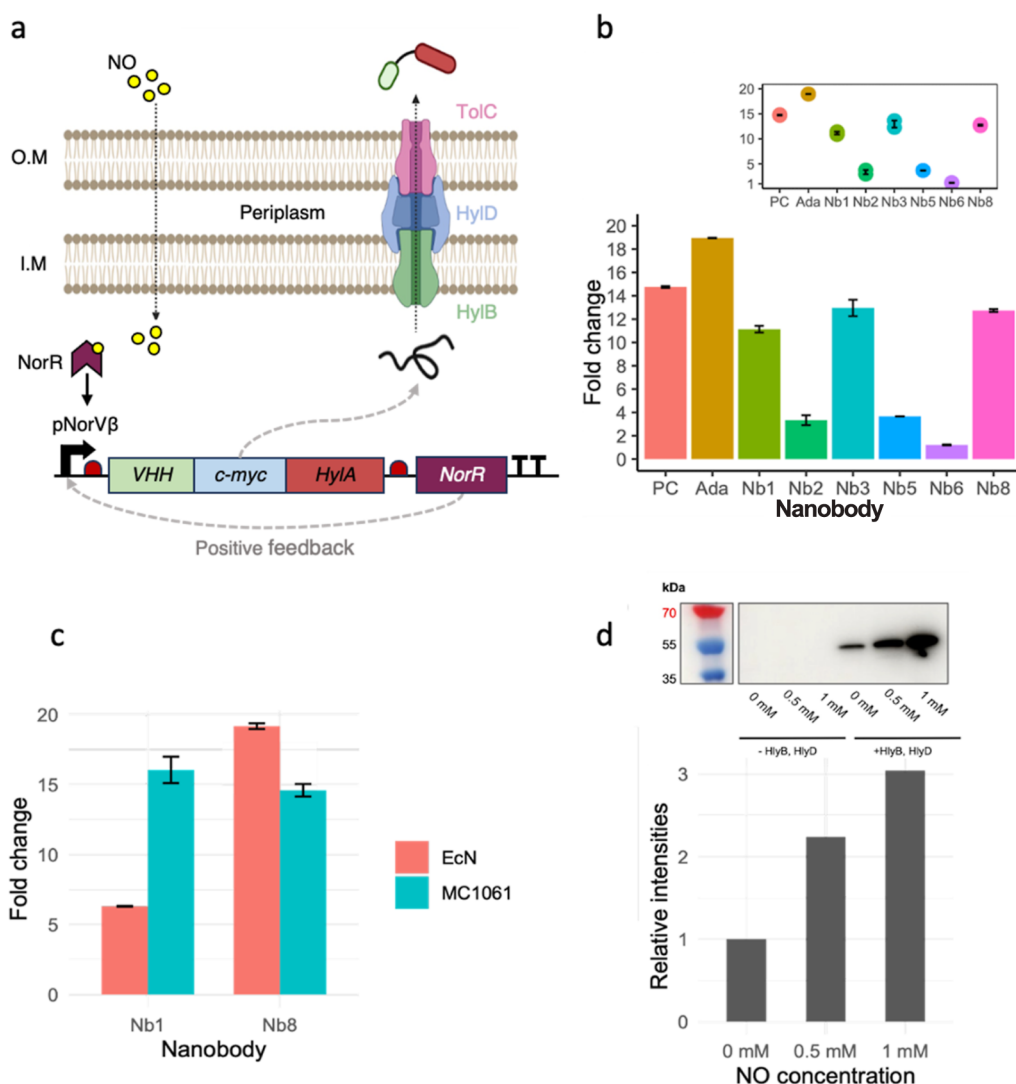


**Figure 3.** Design and characterization of arabinose- and NO-induced anti-TNF $\alpha$  nanobodies secretion in *E. coli Nissle 1917* and *E. coli MC1061*. (a) Principle of NO-induced nanobody secretion with the hemolysin A secretion system. NO is a small organic molecule able to surpass the double membrane of *E. coli*. NO binding to the PnorV- $\beta$  promoter induces the expression of the monovalent nanobody candidate Nb1, which is tagged with a myc- and HlyA-tag. NorR expressions result in a positive feedback loop, enhancing the nanobody expression further. Thanks to the HlyA-tag, the produced nanobodies are secreted by the hemolysin A secretion system in a one-step manner into the extracellular space. (b) Arabinose-induced secretion of monovalent and bivalent nanobodies with *E. coli MC1061*. Western blot and ELISA analysis revealed successful secretion of functional monovalent and bivalent nanobodies upon overnight arabinose induction in *E. coli MC1061*. (c) Arabinose-induced secretion of monovalent and bivalent anti-TNF $\alpha$  nanobodies in *EcN* and *MC1061*. ELISA analysis shows a successful secretion of functional monovalent Nb1 and bivalent Nb8 nanobodies upon overnight arabinose induction, retaining their TNF $\alpha$ -binding capabilities regardless of the HlyA-tag. (d) NO-induced secretion of monovalent anti-TNF $\alpha$  nanobodies with a single-RBS system in *E. coli MC1061*. The NO-induced monovalent nanobody secretion was achieved using the single-RBS system ( $\beta$ -1). This yielded a more dynamic response to NO than the previous two-RBS system ( $\beta$ -2) (Figure S16) and a lower baseline expression of monovalent nanobody candidate Nb1 in *E. coli MC1061*. The absence of the two secretion system components (HlyB and HlyD) resulted, as expected, in no secretion of nanobodies. With increasing NO levels, higher nanobody expression can be observed. A baseline expression in the absence of NO is still present yet weaker than in the  $\beta$ -2 system (Figure S16).

variations in NO levels, as measured by changes in sfGFP fluorescence. The percentage change in sfGFP fluorescence intensity is calculated when the NO concentration shifts from an initial baseline to a new value. This percentage is then normalized against the initial NO concentration, providing a relative measure of change.

**Purified Monovalent and Bivalent Anti-TNF $\alpha$  Nanobodies Efficiently Capture TNF $\alpha$ , Comparable to Monoclonal Antibodies Used in the Clinics.** To develop the nanobody production module, we have selected three previously described anti-TNF $\alpha$  humanized nanobody candidates<sup>42</sup> and combined these to additionally produce bivalent

nanobodies, linked via a short peptide linker (EPKTPKQP-PAAA; for monovalent and bivalent nanobodies see [Materials and Methods, Table 3](#)). First, to assess the proper expression and activity of our candidates, we cloned their sequences into the pSBinit<sup>58</sup> expression vector (see [Materials and Methods, Table 2](#) and [Figures S6 and S7](#)), allowing controlled expression upon L-arabinose induction (see [Figure 2a](#)). We transformed the plasmids into the expression strain *E. coli MC1061* (see [Materials and Methods, Table 1](#)). After induction, we performed periplasmic extraction for monovalent nanobodies and whole-cell lysis for bivalent constructs ([Figure 2a](#)) and observed a quantitatively higher output of monovalent

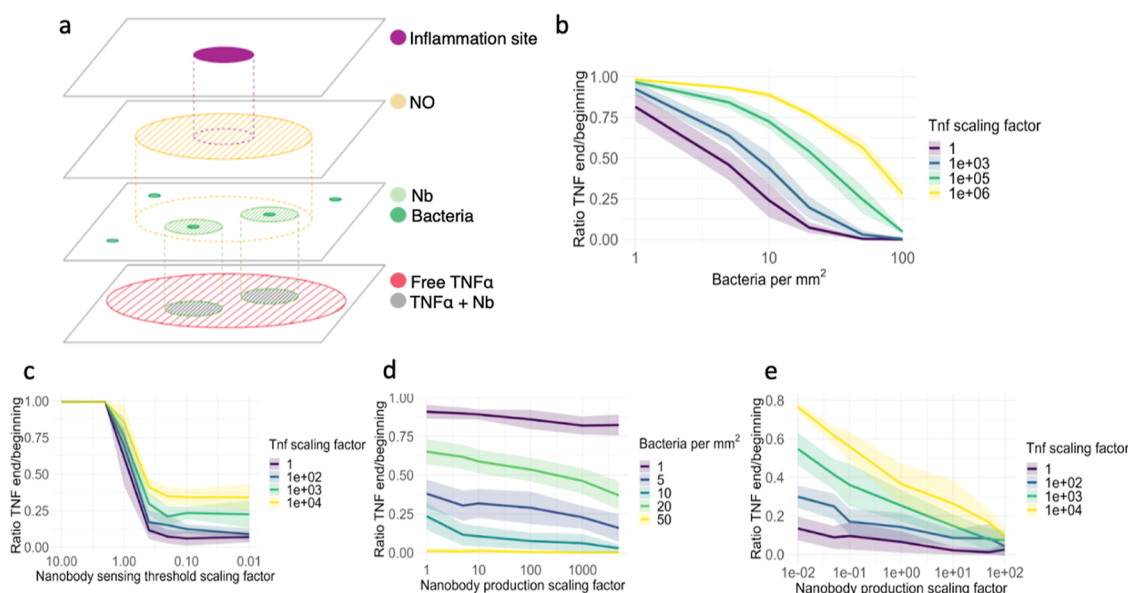


**Figure 4.** Reaction-diffusion model was evaluated on key parameters. The model's purpose was to explore which parameters could be essential for the efficacy of our system. We set parameters that were not varied to their default values, except for the sensing threshold, which we decreased by a factor of 10 during simulations as done in a recent study,<sup>38</sup> for visibility reasons. We simulated each parameter configuration 10 times. Line shadings represent the standard deviation. (a) Illustration of the components of the reaction-diffusion model. (b) Relationship between bacterial density and TNF $\alpha$  concentrations. ( $n = 240$ ). (c) Relationship between sensing threshold and TNF $\alpha$  concentrations. ( $n = 280$ ). (d) Relationship between nanobody production and bacterial density. ( $n = 300$ ). (e) Relationship between nanobody production and TNF $\alpha$  concentrations. ( $n = 380$ ).

nanobodies compared to the bivalent constructs (Figures S8 and S9).

We proceeded by performing an enzyme-linked immunosorbent assay (ELISA) with the purified nanobodies to test their capability to bind TNF $\alpha$  (see Materials and Methods). The Figure 2b shows the fold change in the binding capacity of our different nanobody candidates compared to our negative control. The bivalent nanobodies exhibit a statistically significant enhancement in binding efficiency, demonstrating an average 1.3-fold increase over the monovalent nanobodies (see Figure S10). The bivalent constructs show a mean TNF $\alpha$  binding capacity of  $13.5 \pm 0.1$  (mean  $\pm$  s.d.), compared to  $12.3 \pm 0.2$  for the monovalent constructs. Adalimumab, an approved monoclonal anti-TNF $\alpha$  antibody that is already used in the clinic to treat IBD (see Materials and Methods for antibody purification), is used as a positive control and our bivalent nanobody constructs show a similar binding capability to this therapeutic.

**Anti-TNF $\alpha$  Nanobodies Show Anti-inflammatory Effects on Stimulated Human Monocytes In Vitro.** To evaluate the effect of anti-TNF $\alpha$  nanobodies on the immune response of cells to an inflammatory stimulus in vitro, we stimulated THP-1 human monocytes with increasing concentrations of recombinant TNF $\alpha$  (rTNF $\alpha$ ) and subsequently added our purified nanobody candidates (see Materials and Methods). We performed real-time quantitative PCR analysis and measured the relative amount of *IL1B* expressed by immune cells as a response to inflammation through TNF $\alpha$  signaling (Figure 2c, Supporting Information Methods). The cytokine IL-1 $\beta$  is an important inflammation mediator and, therefore, a good marker to prove functional TNF $\alpha$ -inhibition.<sup>59</sup>

We were able to observe an up to 4-fold decrease in *IL1B* expression of stimulated monocytes when different nanobodies

were added compared to the control cells that only received the inflammatory stimulus (Figure 2d). This experiment shows that tested nanobodies have the same capability to lower inflammation as monoclonal antibodies, which are already used in the clinic to treat IBD patients. However, with increasing TNF $\alpha$  concentrations, the anti-inflammatory effect that the nanobodies have on the monocytes seems to slowly decline, indicating that higher concentrations of nanobodies are required to maintain low *IL1B* expression levels. This decline is not observable with the available drug Adalimumab.<sup>60</sup> It is also important to note that the difference between monovalent and bivalent nanobody constructs does not seem to be of great influence on the inflammatory response of triggered monocytes.

**Anti-TNF $\alpha$  Nanobodies Can Be Secreted from EcN.** In order for EcN to deliver nanobodies to its environment, it must be able to secrete them without impacting their function. To achieve this, we engineered the HlyA secretion system<sup>47,48</sup> into EcN and fused the nanobodies to the HlyA-tag, marking them for selective export (Figures 3a and S11). As a first step, we tested the functionality of the nanobodies after expression and secretion in *E. coli* MC1061. We performed a double transformation of *E. coli* MC1061 with two plasmids: our secretion plasmid (Figure S11) and the pSBinit expression plasmid, which allows for nanobody expression upon L-arabinose induction (Figure S7). After overnight induction, we harvested the supernatant from the cell culture, and performed a Western blot and ELISA to quantify the presence and TNF $\alpha$  binding of the secreted nanobodies (Figure 3b). In EcN, the nanobody Nb1 and the bivalent nanobody Nb8 were successfully secreted, and their binding affinities were maintained (Figures 3c and S13 and S14).

**NO Can Be Used to Trigger Anti-TNF $\alpha$  Nanobody Expression.** To create a system capable of sensing NO and

thereby triggering the production and secretion of nanobodies, we built a new plasmid, where we cloned the monovalent nanobody Nb1 downstream of the aforementioned pNorV $\beta$  promoter (see Table 2, Supporting Information Methods and Figure S15). We used the circuit with two RBS ( $\beta$ -2) upstream of the cloned nanobodies, as it presented the highest expression levels. We used DETA/NO for induction, allowing cells to express nanobodies overnight. We then quantified the presence of nanobodies in the supernatant by Western blot, in which we detected secreted nanobodies using a C-terminal myc-tag. The Western blot showed that while EcN could sense NO and increase the expression and secretion of anti-TNF $\alpha$  nanobodies, there was still a high-level baseline expression without NO (see Figure S16).

Despite the high levels of baseline expression, the secreted nanobodies maintained their functionality, as shown in ELISA assays (see Figure S16). To reduce baseline expression, we tested an alternative circuit differing by having a single RBS ( $\beta$ -1) upstream of the nanobody coding region. This architecture had previously shown less expression leakage. The single RBS system yielded a more dynamic response to NO concentration in *E. coli* MC1061 after 8 h of expression. Relative expression showed a 3-fold increase from baseline to a 1 mM NO concentration (Figure 3d). It is worth noting that we observed a basal production of nanobodies even without the addition of the NO inducer (Figure 3d, rightmost Western blot and its corresponding bar plot). Lastly, the control with no secretion system does not present nanobodies in the supernatant. This observation confirms the need for a secretion system to export the nanobodies, as cell death does not appear to result in the release of functional nanobodies.

**Coarse-Grained Model for Engineered Probiotics in the Gut.** To support the experimental claims, we constructed a two-dimensional lattice-based reaction-diffusion model<sup>61–65</sup> of the gut environment, as in vivo testing in the gut microbiome is outside the scope of this study. The model is illustrated in Figure 4a.

The model's primary objective was to examine the interactions between EcN and inflammation sites in a simplified manner, specifically focusing on NO concentrations,<sup>36</sup> the production rates of TNF $\alpha$ <sup>66</sup> and the bacterial response to NO through the production of the TNF $\alpha$ -binding nanobodies.<sup>67</sup> Model methods and an in-depth description of the parameters used can be found in the Model Supporting Information Methods section of the appendix. Through cycles of diffusion, decay, and reemission, we provided a preliminary outlook on the efficacy of our proposed treatment and its potential for healthcare applications. We note that the model is a coarse-grained one and faithfully representing the gut environment was out of its scope. We focused on identifying the crucial parameters to tune in future work to optimize the treatment before heading into a further testing stage.

To favor interpretability, generalization, and to promote ease of access and collaboration, the model follows a simplicity-based design. The model interprets a 1 mm<sup>2</sup> area of the gut surface as a 2D grid, with each grid cell representing a 1  $\mu$ m<sup>3</sup> volume containing the local concentration values for each parameter. The model operates in discrete time steps, with adaptations to make it approach a continuous time scale.

**Estimating the Minimum Number of Bacteria for Effective Treatment.** To get an overview of the importance of the different parameters, we performed a series of simulations where we swept two variables at the same time

over the range of our expected values and simulated for 60 s time steps.

In our first series of simulations, illustrated in Figure 4b, we estimated the minimum number of bacteria needed to provide effective treatment and evaluated the densities on a great range of biologically plausible TNF $\alpha$  concentrations. The results show that around 20 bacteria per mm<sup>2</sup> should be enough to cover the inflamed gut area and sufficiently combat the inflammation for the expected TNF $\alpha$  concentrations. For higher concentrations of TNF $\alpha$ , however, the nanobodies produced are not sufficient to combat inflammation, and larger bacterial populations are needed. The graphs suggest a rough relationship of a doubling in bacterial density being able to combat a magnitude higher TNF $\alpha$  concentration. Bacterial density estimates place this requirement at a feasible replacement value of 20 out of 10<sup>4</sup> gut bacteria per mm<sup>2</sup>.<sup>68,69</sup> Therefore, we assume that the necessary colonization threshold is attainable and will be reached in further experiments. In Figure 4e, we investigate whether increasing the nanobody production could also be a viable solution.

**NO Detection Threshold and Nanobody Production.** In our study, the threshold for NO detection, the minimum amount of NO required for nanobody production, is essential for ensuring an inflammation-dependent response. In Figure 4c, we evaluated a range of these sensing thresholds and the amount of TNF $\alpha$  at the inflammation sites. As our threshold closely aligns with the expected NO concentration of around 15  $\mu$ M<sup>36</sup> (for details, see Supporting Information Methods and Figure S17), even slight decreases in sensitivity lead from the absence of inflammation reduction to complete reduction, even with higher than expected amounts of TNF $\alpha$ . Increased sensitivity of the bacteria toward NO gives diminishing returns, as this mainly affects bacteria in edge regions that detect trace amounts of NO but do not produce nanobodies at the affected location. In turn, there will be an excess production of nanobodies in these regions that hardly contribute to combating inflammation. It is important to note that in our simulations, we kept the amount of NO produced at inflammation sites constant, even for higher TNF $\alpha$  concentrations. In a patient setting, however, NO levels might vary significantly.

**Comparison between Bacterial Number and Nanobody Production.** In Figure 4d, we assessed the importance of the number of bacteria we can introduce against the nanobody production of a single bacteria. For our expected TNF $\alpha$  values, the number of bacteria has a far greater effect than the amount of nanobodies produced per bacteria. This is most likely due to the nanobodies being spread locally, and even at the same amount of net nanobodies produced, greater coverage of gut-inflamed areas ensures that the nanobodies are produced where they need to be. This trade-off also guarantees that no excess amount of nanobodies is produced which could lead to possible side effects. In vivo testing is required to assess the actual viability of our engineered bacteria, and further optimization should be based on this.

In Figure 4e, we investigate whether higher TNF $\alpha$  concentrations can be mitigated by increasing nanobody production. The results demonstrate that, with a bacterial density of at least 20 per mm<sup>2</sup>, an increase in nanobody production effectively reduces TNF $\alpha$  levels. However, this effect is less pronounced compared to increasing the number of bacteria, as shown in Figure 4b, which more effectively reduces even higher concentrations of TNF $\alpha$ . Nevertheless,

increasing nanobody production might be easier to achieve and still offers a viable approach to combating elevated TNF $\alpha$  concentrations.

## DISCUSSION

Here, we describe the development of an integrated molecular system in EcN for the local sensing of gut inflammation and the production/delivery of high-specificity effectors to mitigate such inflammation. Specifically, we have engineered both laboratory and nonpathogenic/probiotic human *E. coli* strains with a coupled system that can secrete nanobodies in a regulated manner upon NO induction. Secretion is achieved through the adoption of an exogenous type I hemolysin A secretion system, which has been characterized in EcN for the first time in this study. We have also characterized a new library of humanized nanobodies in EcN, demonstrating that they can be successfully secreted and retain their functionality in vitro and in cell assays, binding to TNF $\alpha$  as efficiently as conventional drugs used for targeting this pro-inflammatory molecule. Modularity is a key strength of our system. The regulator can be easily swapped, allowing the detection of different biomarkers.<sup>27,34</sup> The cargo (nanobody in our case) can also be replaced in a straightforward manner with other therapeutic proteins, such as small peptides and colonization-increasing factors.

Although mathematical models regarding gut colonization are available,<sup>70–74</sup> they are primarily focused on host–pathogen interactions and not on the colonization-sensing-delivery process from engineered probiotics. Thus, we also developed a simplified yet insightful modeling framework to investigate relevant parameters in probiotic engineering and its subsequent colonization in the gut. Specifically, we investigated the interactions between the probiotic bacteria and inflammation sites, focusing on biomarker (NO) concentration detection thresholds, therapeutic molecule production rates (TNF $\alpha$ ), and the bacterial response in terms of therapeutic–target interactions (nanobody–TNF $\alpha$ ). We observed that approximately 20 bacteria per mm<sup>2</sup> are sufficient to manage inflammation. Bacterial density estimates place this requirement at a feasible replacement value of 20 out of 10<sup>4</sup> gut bacteria per mm<sup>2</sup>.<sup>68,69</sup> However, at higher TNF $\alpha$  levels, increased bacterial densities are necessary, suggesting a rough doubling of bacterial density for each magnitude increase in TNF $\alpha$  concentration.

The current understanding of NO concentrations at inflammation sites within the gut across various patient demographics is limited, with most data based on serum concentrations.<sup>36</sup> It is estimated that a baseline concentration of around 14  $\mu$ M NO is typically necessary to detect gut inflammation.<sup>36</sup> However, we anticipate that the luminal NO concentrations in the gut, particularly at sites of active inflammation, are likely to be considerably higher than this threshold. This expectation is based on the fact that NO, with its notably short half-life and rapid diffusion rates within the body,<sup>75,76</sup> would be more concentrated in regions immediately adjacent to inflammation sites. Given the scarce available data on serum NO concentrations,<sup>36</sup> our simulations suggest that an optimal concentration for nanobody production in response to NO is approximately 15  $\mu$ M. We also observed that enhancing bacterial sensitivity to NO beyond this threshold may lead to diminishing returns. Specifically, this could result in the overproduction of nanobodies in peripheral areas, where

they might not contribute effectively to inflammation reduction.

When comparing the impact of the bacterial number on nanobody production per bacterium through simulations, our results indicate that the number of bacteria plays a more critical role than the number of nanobodies produced by each bacterium. This is likely due to the localized distribution of nanobodies, suggesting that a broader gut coverage by bacteria is more effective than increasing the production rate of nanobodies per bacterium. This balance is crucial to avoid the production of excess nanobodies, which could lead to potential side effects and metabolic burden on the bacterial host.<sup>77–79</sup> We highlight that a mathematical model is an oversimplification of reality and does not capture many complexities of the in vivo environment. Future developments in our modeling approach should include important variables such as the consequences of gene expression noise (heterogeneity in gene expression),<sup>80,81</sup> the reevaluation of the assumptions regarding gut geometry, an enhancement of the diffusion model to encompass three dimensions and the consequences of microenvironmental gut conditions on bacterial growth.<sup>82</sup> Moreover, conducting in vivo studies of the treatment will be instrumental in refining the model as this iterative process of model refinement is essential for advancing our understanding of engineered probiotics.<sup>83,84</sup>

The experimental characterization of our NorR-based circuit revealed that the NO detection threshold in our constructs was higher than the one reported in the original study where this circuit was designed.<sup>38</sup> This discrepancy could stem from several factors. First, the plasmid used in our experiments differed from that in the referenced study,<sup>38</sup> and we were unable to access the complete sequences of their constructs, which may have influenced our results. Additionally, our experiments were conducted under aerobic conditions. Previous research has shown that anaerobic environments, akin to the gut's natural state, can decrease the NO detection threshold of the NorR system by at least 5-fold, due to interactions between oxygen and the iron center of NorR.<sup>49</sup> Consequently, while our sensor system in EcN has been characterized and improved under aerobic conditions, there is substantial potential to enhance its sensitivity to lower, more physiologically relevant NO concentrations. Future studies could achieve this through advanced protein and promoter engineering techniques (e.g., directed evolution and combinatorial designs coupled with fluorescence-based screening methods<sup>85–88</sup>) and by transitioning to anaerobic assays.

We highlight that although our results support the potential of our system for biotherapeutic applications, the transition from test tubes to translational applications faces many challenges,<sup>89–92</sup> from consistent therapeutic delivery methods to the long-term maintenance of engineered bacteria in the gut. The stable colonization of engineered probiotics in the gut can be negatively impacted by metabolic burden—the allocation of resources toward the engineered system—which can hinder bacterial growth in the complex microbiome environment.<sup>78</sup> Moreover, evolutionary changes might disrupt circuit functionality over short time periods.<sup>93</sup> The heterogeneity in bacterial expression due to background genetic mutations or expression noise might also lead to variability in treatment efficacy.<sup>93</sup> Additionally, the interactions between the host immune system and engineered probiotics require thorough investigation to ensure long-term efficacy and safety.<sup>94,95</sup> To address some of these challenges, strategies such as integrating the genetic



Table 1. List of Bacterial Strains Used in This Study

name	genotype	selective antibiotics	T, °C	description
<i>E. coli</i> Nissle 1917	unavailable	none	37 °C	first described on refs 15 and 16. obtained from Mutaflor (Herdecke, Germany)
<i>E. coli</i> MC1061	F <sup>-</sup> <i>hsdR</i> (r <sub>K</sub> <sup>-</sup> , m <sub>K</sub> <sup>+</sup> ) <i>araD</i> 139 Δ( <i>araABC-leu</i> )7679 <i>galU galK</i> Δ <i>lacX74 rpsL</i> (StrR) <i>thi mcrB</i> /P3: Kan <sup>R</sup> Amp <sup>R</sup> (am) Tet <sup>R</sup> (am)	streptomycin, kanamycin, ampicillin, tetracycline	37 °C	commercially obtained from Thermo Fisher (C66303)
<i>E. coli</i> Mach1	F <sup>-</sup> <i>φ80lacZΔM15</i> Δ <i>lacX74 hsdR</i> (r <sub>K</sub> <sup>-</sup> , m <sub>K</sub> <sup>+</sup> ) Δ <i>recA</i> 1398 <i>endA1 tonA</i>	none	37 °C	commercially obtained from Thermo Fisher (C862003)

Table 2. List of Plasmids Used in This Study

name	description
piGEM1	this study. negative control. encodes for <i>sfGFP</i> and <i>norR</i> , does not contain any promoter
piGEM3	this study. encodes for <i>sfGFP</i> and <i>norR</i> under the control of the already characterized inducible promoter pNorV
piGEM2.1	this study. encodes for <i>sfGFP</i> and <i>norR</i> under the control of the inducible promoter pNorVβ. this construct contains 1 RBS directly upstream of <i>sfGFP</i>
piGEM2.2	this study. encodes for <i>sfGFP</i> and <i>norR</i> under the control of the inducible promoter pNorVβ. this construct contains 2 RBS and a spacer upstream of <i>sfGFP</i>
piGEM2.3	this study. encodes for <i>sfGFP</i> and <i>norR</i> under the control of the inducible promoter pNorVβ. this construct contains 3 RBS and a spacer upstream of <i>sfGFP</i>
piGEM2.2N	this study. encodes for <i>sfGFP</i> under the control of the inducible promoter pNorVβ. this construct contains 2 RBS and a spacer upstream of <i>sfGFP</i> . this construct does not contain <i>norR</i>
pSBinit	retrieved from ref 58, addgene #110100. <i>E. coli</i> entry and expression vector for FX cloning system, N-terminal pelB signal sequence and C-terminal myc and 6× HisTag
purNb1	this study. nanobody candidate VHH#2B cloned into pSBinit expression vector via FX cloning
purNb2	this study. nanobody candidate VHH#3E cloned into pSBinit expression vector via FX cloning
purNb3	this study. nanobody candidate VHH#12B cloned into pSBinit expression vector via FX cloning
purNb4	this study. nanobody candidate VHH#2B–VHH#2B cloned into pSBinit expression vector via FX cloning
purNb5	this study. Nanobody candidate VHH#3E–VHH#3E cloned into pSBinit expression vector via FX cloning
purNb6	this study. nanobody candidate VHH#12B–VHH#12B cloned into pSBinit expression vector via FX cloning
purNb7	this study. nanobody candidate VHH#2B–VHH#3E cloned into pSBinit expression vector via FX cloning
purNb8	this study. nanobody candidate VHH#2B–VHH#12B cloned into pSBinit expression vector via FX cloning
purNb9	this study. nanobody candidate VHH#3E–VHH#12B cloned into pSBinit expression vector via FX cloning
pSS	this study. plasmid encoding HlyB and HlyD required for the HlyA secretion system under a constitutive promoter (J23100). Contains chloramphenicol resistance gene
pNb	this study. plasmid encoding HlyA and myc-tag under inducible pBad promoter with restriction sites allowing the cloning of the different nanobodies in front of the two tags. Contains ampicillin resistance gene
pNb1	this study. nanobody candidate VHH#2B cloned into pNb plasmid via FX cloning
pNb2	this study. nanobody candidate VHH#3E cloned into pNb plasmid via FX cloning
pNb3	this study. nanobody candidate VHH#12B cloned into pNb plasmid via FX cloning
pNb5	this study. nanobody candidate VHH#3E–VHH#3E cloned into pNb plasmid via FX cloning
pNb7	this study. nanobody candidate VHH#2B–VHH#3E cloned into pNb plasmid via FX cloning
pNb8	this study. nanobody candidate VHH#2B–VHH#12B cloned into pSBinit expression vector via FX cloning
pNO1_Nb1	this study. nanobody candidate VHH#2B cloned into piGEM2.1 plasmid via Gibson
pNO3_Nb1	this study. nanobody candidate VHH#2B cloned into piGEM2.3 plasmid via Gibson

circuit into the genome can enhance the stability and robustness of the device's functionality.<sup>77,93</sup> Combining whole-cell and host-microbiome metabolic models with in vivo assays of viability and prevalence of engineered probiotics is also important for predicting the long-term maintenance of such systems.<sup>92,96–100</sup> Moreover, incorporating antibiotic resistance-free plasmids<sup>101</sup> and containment modules<sup>92,102</sup> is important to prevent the unintended spread of engineered bacteria and antibiotic resistance genes.

Despite the aforementioned challenges, synthetic biology is rapidly transitioning from laboratory experiments to tangible, real-world applications.<sup>103–105</sup> In 2019, ZBiotics Company, USA, pioneered this field by being the first to produce and sell genetically engineered probiotic products, marking the beginning of a burgeoning industry. In a recent notable study, researchers developed a novel system within EcN (PROT3EcT) and validated it in an animal model.<sup>33</sup> They demonstrated effective mouse gut colonization with con-

stitutive production of nanobodies targeting TNFα, resulting in localized inflammation mitigation. Although our system employs different components—specifically, a biomarker-dependent sensing module, distinct nanobodies, and an alternate secretion system—their results are highly encouraging, suggesting the potential functionality of our system in animal models. In this rapidly progressing landscape, our study focused on providing new parts, a new modular system, and a mathematical framework to expand EcN's synthetic biology toolbox and support ongoing efforts in the probiotic engineering community.

## ■ MATERIALS AND METHODS

**Media and Buffers.** M9 medium is advantageous due to its low cost, low autofluorescence (when excited at 488 nm), and low absorbance. We used M9 medium, supplemented with specific amino acids or other metabolites (such as thiamine or casamino acids), for experiments measuring sfGFP fluores-

cence to ensure minimal autofluorescence and absorbance of the samples. To prepare a 50 mL volume of M9 medium, we added the reagents in the following order: 10 mL of M9 salt (5×), 100  $\mu$ L of MgSO<sub>4</sub> (1 M), 50  $\mu$ L of CaCl<sub>2</sub> (0.1 M), 1.5 mL of Cas Aa (2%), and 1 mL of glucose (20%), then added water to reach a final volume of 50 mL. If necessary, we supplemented M9 medium with the appropriate antibiotic at a 1:1000 ratio. We conducted all preparation steps under sterile conditions.

**Table 3. Nanobodies Used in This Study**

Nb ID	mono or bivalent	Nb parts	reference
Nb1	monovalent	VHH#2B	patent <sup>42</sup>
Nb2	monovalent	VHH#3E	patent <sup>42</sup>
Nb3	monovalent	VHH#12B	patent <sup>42</sup>
Nb4	bivalent	VHH#2B	patent <sup>42</sup>
Nb5	bivalent	VHH#3E	patent <sup>42</sup>
Nb6	bivalent	VHH#12B	patent <sup>42</sup>
Nb7	bivalent	VHH#2B + VHH#3E	patent <sup>42</sup>
Nb8	bivalent	VHH#2B + VHH#12B	patent <sup>42</sup>
Nb9	bivalent	VHH#3E + VHH#12B	patent <sup>42</sup>

**Plate Reader Fluorescence Assay.** To measure the activity of all constructs, we transformed plasmids into *E. coli Nissle 1917*. We grew freshly plated single colonies in LB medium supplemented with ampicillin and incubated cultures at 37 °C and 220 rpm. On the day of the assay, we spun down the bacteria from the overnight cultures, resuspended them in M9 medium supplemented with ampicillin (M9-Amp) and diluted cultures to OD<sub>600</sub> = 0.5. We then assayed the cultures (20  $\mu$ L) in a 96-well microplate with 170  $\mu$ L of M9-Amp and 10  $\mu$ L of the different compounds tested. We used five different concentrations (8, 31, 125, 500 and 2000  $\mu$ M) of the NO donor diethylenetriamine/NO (DETA/NO) diluted in ddH<sub>2</sub>O as the inducer. We quantified cell growth (OD<sub>600</sub>) and sfGFP fluorescence using a Tecan Spark 10 M plate reader. We calculated the responsiveness of the genetic circuit as arbitrary units using the ratio between fluorescence levels and the optical density at 600 nm (reported as sfGFP/OD<sub>600</sub>) after background correction. As a control for the inducer, we also measured all constructs in the absence of DETA/NO. As a control for cellular autofluorescence background, we also assayed *E. coli Nissle 1917* transformed with the same plasmid but without a promoter to drive sfGFP expression. We measured fluorescence and absorbance at 10 min intervals for 16 h at 37 °C and under constant shaking (orbital shaking, 0.1 mm orbital averaging). We performed all experiments in technical and biological triplicates. We processed raw data using an ad hoc R script (<https://www.r-project.org/>).

**Flow Cytometry Analysis.** We conducted a high-throughput single-cell analysis of bacteria containing variants of the NO detection module and a negative control plasmid (promoterless *sfGFP*) as follows: first, we selected single colonies of the transformed strain (*EcN*) and cultivated them overnight in LB medium supplemented with ampicillin at 37 °C and 220 rpm. Next, we diluted overnight-grown cells in a ratio of 1:10 in fresh LB and grew them overnight at 37 °C and 220 rpm with different concentrations of the DETA/NO inducer (0, 1, 1.5, 2 mM). We diluted overnight-grown cells in a ratio of 1:100 in 1 mL of filtered cold Dulbecco's PBS (Sigma-Aldrich #D8537) in 15 mL FACS tubes and immediately stored them on ice to halt metabolic processes.

We set measurements on a BD FACSCantoII machine with the BD FACSDiva 6.1.3 Software after calibration with both CS&T IVD beads and Rainbow Calibration beads (8 peaks, 107/mL, 3.0–3.4  $\mu$ m, RCP-30-5A) for conversion of arbitrary fluorescence units into MEFL. Excitation and emission filters utilized were 488 nm and 530/30 nm, respectively. We adjusted side-scatter and forward-scatter PMT voltages using bacteria from the negative control, until the distribution of each parameter was centered on the scale. We adjusted FITC/GFP PMT voltage using bacteria from the positive control until the upper edge of the “bell curve” from the fluorescent population was 1 order of magnitude below the upper end of the scale. We acquired a total of 50,000 events for each biological triplicate and washed cells with PBS before measuring when the bacterial density was too high to avoid the formation of aggregates.

**Nanobodies Purification.** We transformed *E. coli MCI061* with the pSBinit plasmids containing our 9 different nanobody candidates. The expression vector contains an FX cloning site where we insert our ordered nanobody fragments. The C-terminal myc and 6× His-tags are included on the plasmid backbone and automatically added in case of a successful FX cloning (Figure 2a). We grew the cells in 600 mL liquid cultures (1:1000 dilution of antibiotic) at 37 °C until an OD of 0.4 to 0.7 was reached. We then induced the expression by the addition of 0.02% L-arabinose and allowed bacteria to express the nanobodies for 16 h at 22 °C. We spun down cells at 4,500 rpm for 15 min at 4 °C and transferred the resulting supernatant to a bottle with 20 nM imidazole pH 7.5. To extract the nanobodies from the solution, we performed a batch binding using 5 mL Ni-NTA resin for 2 h while shaking. We poured the resin into gravity flow columns and washed them with Tris-buffered saline (TBS) pH 7.5, 30 mM imidazole. We eluted nanobodies with 10 mL TBS pH 7.5 and 30 mM imidazole and collected them into fractions, which we measured with the NanoDrop spectrophotometer (Thermo Fisher Scientific). We pooled the fractions with low concentrations and further concentrated them using concentration columns (spun at 2,500g in 10 kDa concentrators). Lastly, we loaded the purified nanobody candidates on the Sepax in TBS (pH 7.5).

**Cultivation of THP-1 Nonadherent Human Monocytes.** We substituted growth medium (RPMI 1640, Gibco) with 10% fetal bovine serum (FBS) and stored at 4 °C. We maintained cell densities between 0.1 and 1.0  $\times 10^6$  cells/mL, splitting them at a ratio of 1:2 or 1:3 (approximately 0.5  $\times 10^6$  cells/mL) every 3 to 4 days. THP-1 cells display a doubling time of roughly 35–50 h. During splitting, we transferred cells into 50 mL falcon tubes and centrifuged them at 1700 rpm for 5 min. We removed the supernatant and resuspended cells in fresh media. After counting the cells, we seeded them at the optimal density.

**Cell Assay.** Before the beginning of the actual cell assay, we centrifuged THP-1 cells and resuspended them in starvation media (RPMI 1640 without FBS) and seeded at a density of 1  $\times 10^6$  cells/mL in a 96-well plate (final volume: 200  $\mu$ L). We then incubated cells for 24 h at 37 °C with 5% CO<sub>2</sub>, according to the cell-specific cultivation protocol.

The next day, we prepared a TNF $\alpha$  dilution series (100, 50, 10, 5, 1, 0.5, 0.1 ng/mL) and kept them on ice. Additionally, we diluted the nanobodies to a final concentration of approximately 100 nM and stored them on ice. After starving the cells for 24 h, we added the diluted nanobodies to the well

plate and gently shook the plate before incubating it for 30 min. Afterward, we stimulated the cells with rTNF $\alpha$  and incubated them for 24 h at 37 °C with 5% CO<sub>2</sub>. We then harvested the cells, transferred them to Eppendorf tubes, and centrifuged them at 3.5g for 10 min at 4 °C. After removing the supernatant, we froze the cell pellet with liquid nitrogen and stored it at –80 °C for further quantitative RT-qPCR analysis.

#### Induction of Nanobody Production and Secretion.

We inoculated successfully double-transformed bacteria in 5 mL precultures with a 1:1000 antibiotic dilution and incubated them at 37 °C overnight while shaking at 120 rpm. The next day, we transferred the cells to 10 mL TB with a 1:1000 antibiotic dilution and grew them at 37 °C while shaking until an OD<sub>600</sub> of approximately 0.6 was reached. To induce secretion, we added either L-arabinose (final concentration: 0.02%) or DETA/NO (testing different concentrations), depending on the transformed cells and their nanobody plasmid. We incubated the cultures at 37 °C overnight to allow them to express and secrete nanobodies. We then spun down the cells and collected 2 mL of supernatant for testing via Western blot or ELISA.

If we needed to test the cell lysate, we first resuspended the cells in TBS and transferred them to a screw-lid microcentrifuge tube. We added one PCR tube of glass beads and lysed the cells using the maxiprep machine at 4 m/s for 20 s. We placed the cells on ice for 5 min for recovery. We then repeated the shaking process twice, with 5 min rest intervals.

**Enzyme-Linked Immunosorbent Assay.** The night before the experiment, we coated a 96-well Nunc Maxicrop immunoplate with 100  $\mu$ L of protein A solution (1:1000 dilution in PBS) in each well, sealed the plate, and incubated it at 4 °C overnight. Before starting the experiment, we freshly prepared the buffers according to the following specifications for ELISA: TBS at 1 $\times$  concentration; TBS-bovine serum albumin (BSA), which is TBS supplemented with 0.5% BSA (weight/volume); TBS-D, consisting of TBS supplemented with a detergent of choice at an amount equivalent to three times the critical Micelle concentration of the chosen detergent; and TBS-BSA-D, combining TBS with both 0.5% BSA and 0.1% of the chosen detergent (weight/volume).

We washed each well with 250  $\mu$ L TBS and then blocked them with 250  $\mu$ L TBS-BSA for 30 min. We washed the plate three times with 250  $\mu$ L TBS per well. Then, we added 100  $\mu$ L of 1:2000 diluted monoclonal anti-c-myc antibody (diluted in TBS-BSA-D) to each well and incubated for 20 min. We washed the plate three times with 250  $\mu$ L TBS-D and added samples diluted in TBS-BSA-D (20  $\mu$ L in 80  $\mu$ L solvent for supernatant or periplasmic extraction, or approximately 50 nM for purified nanobodies). We washed the plate three times with 250  $\mu$ L TBS-D, then added 100  $\mu$ L of 50 nM biotinylated TNF $\alpha$  in TBS-BSA-D and incubated for 20 min. We washed the plate three times with 250  $\mu$ L TBS-D before adding 100  $\mu$ L of 1:5000 diluted streptavidin-peroxidase polymer solutions (diluted in TBS-BSA-D) and incubating for 20 min. After washing the plate three times with 250  $\mu$ L TBS-D, we added 100  $\mu$ L of ELISA developing buffer and incubated until individual wells turned blue, which took between 5 and 15 min. We then measured the absorbance at 650 nm using a plate reader. ELISA signals as small as 1.5-fold above the background can indicate a high-affinity binder.

## ■ ASSOCIATED CONTENT

### Data Availability Statement

The interactive version of our simulations is available at <https://2022.igem.wiki/uzurich/model>.

### Supporting Information

The Supporting Information is available free of charge at <https://pubs.acs.org/doi/10.1021/acssynbio.4c00036>.

General methods employed in this study include PCR (Section 1.1), real-time quantitative PCR (Section 1.2), preparation of calcium-competent EcN (Section 1.3), heat-shock transformation of calcium-competent EcN (Section 1.4), Gibson assembly (Section 1.5), preparation of electrocompetent EcN (Section 1.6), electroporation (Section 1.7), and Western blot (Section 1.8). The plasmid design and construction cover secretion plasmid design (Section 2.1), NO-sensing plasmid design (Section 2.2), and plasmid cloning (Section 2.3). Model Supporting Information methods include assumptions and parameters (Section 3.1), number of inflammatory sites (Section 3.2), number of bacteria (Section 3.3), emission coefficients (Section 3.4), diffusion coefficients (Section 3.5), emission dynamics (Section 3.6), and diffusion dynamics (Section 3.7). Supporting Information tables list oligonucleotides used (Table S1). Supporting Information figures feature the plasmid map of the negative control (Figure S1), the plasmid map of the engineered NO sensor construct piGEM2 ( $\beta$ -1) (Figure S2), the plasmid map of the engineered NO sensor construct piGEM3 (WT) (Figure S3), the effect of DETA/NO on cellular growth (Figure S4), the impact of removing the plasmid-expressed NorR on NO sensitivity and response strength (Figure S5), the plasmid map of the nanobody purification plasmid (Figure S6), the plasmid map of the arabinose-induced nanobody expression plasmid (Figure S7), the plasmid map of the secretion system plasmid (Figure S8), the plasmid map of the NO-induced nanobody expression plasmid ( $\beta$ -2) (Figure S9), the purification of monovalent and bivalent anti-TNF $\alpha$  nanobodies from *E. coli* MC1061 (Figure S10), the comparison of over day to overnight arabinose-induced nanobody secretion in *E. coli* MC1061 (Figure S11), the arabinose-induced anti-TNF $\alpha$  nanobody production in *E. coli* MC1061 (Figure S12), the arabinose-induced anti-TNF $\alpha$  nanobody production in *E. coli* Nissle 1917 (Figure S13), the analysis of ELISA comparing the binding capabilities of purified and secreted monovalent and bivalent anti-TNF $\alpha$  nanobodies in *E. coli* Nissle 1917 and *E. coli* MC1061 (Figure S14), the NO-induced monovalent anti-TNF $\alpha$  nanobody expression in *E. coli* Nissle 1917 (Figure S15), and a visual comparison between diffusion models (Figure S16) (PDF)

## ■ AUTHOR INFORMATION

### Corresponding Author

Cauã Antunes Westmann – Department of Evolutionary Biology and Environmental Studies, University of Zürich, CH-8057 Zürich, Switzerland; Swiss Institute of Bioinformatics, 1015 Lausanne, Switzerland; [orcid.org/0000-0003-1572-2279](https://orcid.org/0000-0003-1572-2279); Email: [caua.westmann@ieu.uzh.ch](mailto:caua.westmann@ieu.uzh.ch), [caua.westmann@gmail.com](mailto:caua.westmann@gmail.com)

## Authors

Nathalie Weibel – University of Zürich, 8057 Zürich, Switzerland; [orcid.org/0009-0007-1930-5372](https://orcid.org/0009-0007-1930-5372)  
 Martina Curcio – University of Zürich, 8057 Zürich, Switzerland  
 Atilla Schreiber – University of Zürich, 8057 Zürich, Switzerland  
 Gabriel Arriaga – University of Zürich, 8057 Zürich, Switzerland  
 Marine Mausy – University of Zürich, 8057 Zürich, Switzerland  
 Jana Mehdý – University of Zürich, 8057 Zürich, Switzerland  
 Lea Brüllmann – University of Zürich, 8057 Zürich, Switzerland  
 Andreas Meyer – University of Zürich, 8057 Zürich, Switzerland  
 Len Roth – University of Zürich, 8057 Zürich, Switzerland  
 Tamara Flury – University of Zürich, 8057 Zürich, Switzerland  
 Valerie Pecina – University of Zürich, 8057 Zürich, Switzerland  
 Kim Starlinger – University of Zürich, 8057 Zürich, Switzerland  
 Jan DERNIČ – Institute of Pharmacology and Toxicology, University of Zürich, CH-8057 Zürich, Switzerland  
 Kenny Jungfer – Department of Biochemistry, University of Zürich, CH-8057 Zürich, Switzerland  
 Fabian Ackle – Institute of Medical Microbiology, University of Zürich, CH-8006 Zürich, Switzerland; [orcid.org/0000-0002-7199-5004](https://orcid.org/0000-0002-7199-5004)  
 Jennifer Earp – Institute of Medical Microbiology, University of Zürich, CH-8006 Zürich, Switzerland  
 Martin Hausmann – Department of Gastroenterology and Hepatology, University Hospital Zürich and Zürich University, 8091 Zurich, Switzerland  
 Martin Jinek – Department of Biochemistry, University of Zürich, CH-8057 Zürich, Switzerland  
 Gerhard Rogler – Department of Gastroenterology and Hepatology, University Hospital Zürich and Zürich University, 8091 Zurich, Switzerland

Complete contact information is available at:

<https://pubs.acs.org/10.1021/acssynbio.4c00036>

## Author Contributions

<sup>∇</sup>N.W., M.C., A.S., G.A. and M.M. equal contribution. All authors conceived the study and designed experiments. L.B., J.M., M.M., K.J. and C.A.W. carried out NO-induced fluorescent reporter assays, analyzed data, and generated figures. G.A., N.W., F.A. and J.E. carried out nanobody production, purification and activity assays, analyzed data, and generated figures. G.A., N.W., F.A. and J.E. carried out NO-induced anti-TNF nanobodies secretion assays, analyzed data, and generated figures. A.M. and A.S. carried out modeling, simulations, and generated figures. N.W., M.C., A.S., G.A. and M.M., contributed with the writing and editing of the paper. C.A.W. wrote the final version of the paper.

## Funding

This study was supported by multiple funding sources. Academic funding was provided by the University of Zurich through the UZH Alumni Science, the Faculty of Science (MNF), the Faculty of Medicine, the Vice President Research, and the President's Services. Private sponsorship was provided

by Pierre Fabre, Microsynth, the Swiss Academy of Sciences (SCNAT), and Promega. Additionally, this publication was funded by the University of Zurich and the Consortium of Swiss Academic Libraries, making it available as open access.

## Notes

The authors declare no competing financial interest.

## ACKNOWLEDGMENTS

We extend our gratitude to the UZurich 2022 iGEM team for their collective efforts in developing this study. Special thanks to Timothy Kurrer for his support throughout the competition, and to Yen Way Isabell Trinh and Christian Andres Ramos Uria for their insights on our mathematical model. We also thank the UZH flow cytometry facility for their technical support and the gastroenterologists from IBD Net for their feedback. Lastly, we appreciate Professor Markus Seeger, from UZH, for welcoming us in his group, and Professor Richard Murray from Caltech for sharing his expertise and protocols related to *Escherichia coli*Nissle.

## REFERENCES

- (1) Szigethy, E.; McLafferty, L.; Goyal, A. Inflammatory Bowel Disease. *Child Adolesc. Psychiatr. Clin. N.* **2010**, *19* (2), 301–318.
- (2) Guan, Q. A Comprehensive Review and Update on the Pathogenesis of Inflammatory Bowel Disease. *J. Immunol. Res.* **2019**, *2019*, 1–16.
- (3) Ng, S. C.; Shi, H. Y.; Hamidi, N.; Underwood, F. E.; Tang, W.; Benchimol, E. I.; Panaccione, R.; Ghosh, S.; Wu, J. C. Y.; Chan, F. K. L.; Sung, J. J. Y.; Kaplan, G. G. Worldwide Incidence and Prevalence of Inflammatory Bowel Disease in the 21st Century: A Systematic Review of Population-Based Studies. *Lancet* **2017**, *390* (10114), 2769–2778.
- (4) Alatab, S.; Sepanlou, S. G.; Ikuta, K.; Vahedi, H.; Bisignano, C.; Safiri, S.; Sadeghi, A.; Nixon, M. R.; Abdoli, A.; Abolhassani, H.; Alipour, V.; Almasi, M. A. H.; Almasi-Hashiani, A.; Anushiravani, A.; Arabloo, J.; Atique, S.; Awasthi, A.; Badawi, A.; Baig, A. A. A.; Bhala, N.; Bijani, A.; Biondi, A.; Borzi, A. M.; Burke, K. E.; Carvalho, F.; Daryani, A.; Dubey, M.; Eftekhari, A.; Fernandes, E.; Fernandes, J. C.; Fischer, F.; Haj-Mirzaian, A.; Haj-Mirzaian, A.; Hasanzadeh, A.; Hashemian, M.; Hay, S. I.; Hoang, C. L.; Househ, M.; Ilesanmi, O. S.; Jafari Balalami, N.; James, S. L.; Kengne, A. P.; Malekzadeh, M. M.; Merat, S.; Meretoja, T. J.; Mestrovic, T.; Mirzakhimov, E. M.; Mirzaei, H.; Mohammad, K. A.; Mokdad, A. H.; Monasta, L.; Negoi, I.; Nguyen, T. H.; Nguyen, C. T.; Pourshams, A.; Poustchi, H.; Rabiee, M.; Rabiee, N.; Ramezanzadeh, K.; Rawaf, D. L.; Rawaf, S.; Rezaei, N.; Robinson, S. R.; Ronfani, L.; Saxena, S.; Sepehrimanesh, M.; Shaikh, M. A.; Sharafi, Z.; Sharif, M.; Siabani, S.; Sima, A. R.; Singh, J. A.; Soheili, A.; Sotoudehmanesh, R.; Suleria, H. A. R.; Tesfay, B. E.; Tran, B.; Tsoi, D.; Vacante, M.; Wondmieneh, A. B.; Zarghi, A.; Zhang, Z.-J.; Dirac, M.; Malekzadeh, R.; Naghavi, M. The Global, Regional, and National Burden of Inflammatory Bowel Disease in 195 Countries and Territories, 1990–2017: A Systematic Analysis for the Global Burden of Disease Study 2017. *Lancet Gastroenterol. Hepatol.* **2020**, *5* (1), 17–30.
- (5) Zhang, Y.-Z. Inflammatory Bowel Disease: Pathogenesis. *World J. Gastroenterol.* **2014**, *20* (1), 91.
- (6) Cai, Z.; Wang, S.; Li, J. Treatment of Inflammatory Bowel Disease: A Comprehensive Review. *Front Med.* **2021**, *8*, 765474.
- (7) Genaro, L. M.; Gomes, L. E. M.; Franceschini, A. P. M. D. F.; Ceccato, H. D.; de Jesus, R. N.; Lima, A. P.; Nagasako, C. K.; Fagundes, J. J.; Ayrizono, M. D. L. S.; Leal, R. F. Anti-TNF Therapy and Immunogenicity in Inflammatory Bowel Diseases: A Translational Approach. *Am. J. Transl. Res.* **2021**, *13* (12), 13916–13930.
- (8) Sands, B. E.; Kaplan, G. G. The Role of TNF $\alpha$  in Ulcerative Colitis. *J. Clin. Pharmacol.* **2007**, *47* (8), 930–941.

- (9) Rutgeerts, P.; Sandborn, W. J.; Feagan, B. G.; Reinisch, W.; Olson, A.; Johanns, J.; Travers, S.; Rachmilewitz, D.; Hanauer, S. B.; Lichtenstein, G. R.; de Villiers, W. J. S.; Present, D.; Sands, B. E.; Colombel, J. F. Infliximab for Induction and Maintenance Therapy for Ulcerative Colitis. *N. Engl. J. Med.* **2005**, *353* (23), 2462–2476.
- (10) Windsor, J. W.; Kaplan, G. G. Evolving Epidemiology of IBD. *Curr. Gastroenterol. Rep.* **2019**, *21* (8), 40.
- (11) Elhag, D. A.; Kumar, M.; Saadaoui, M.; Akobeng, A. K.; Al-Mudahka, F.; Elawad, M.; Al Khodor, S. Inflammatory Bowel Disease Treatments and Predictive Biomarkers of Therapeutic Response. *Int. J. Mol. Sci.* **2022**, *23* (13), 6966.
- (12) Pedrolli, D. B.; Ribeiro, N. V.; Squizzato, P. N.; de Jesus, V. N.; Cozetto, D. A.; Tuma, R. B.; Gracindo, A.; Cesar, M. B.; Freire, P. J.; da Costa, A. F.; et al. Engineering Microbial Living Therapeutics: The Synthetic Biology Toolbox. *Trends Biotechnol.* **2019**, *37* (1), 100–115.
- (13) Cubillos-Ruiz, A.; Guo, T.; Sokolovska, A.; Miller, P. F.; Collins, J. J.; Lu, T. K.; Lora, J. M. Engineering Living Therapeutics with Synthetic Biology. *Nat. Rev. Drug Discovery* **2021**, *20* (12), 941–960.
- (14) Shan, Y.; Lee, M.; Chang, E. B. The Gut Microbiome and Inflammatory Bowel Diseases. *Annu. Rev. Med.* **2022**, *73* (1), 455–468.
- (15) Nissle, A. Weiteres Über Grundlagen Und Praxis Der Mutaflorbehandlung. *Dtsch. Med. Wochenschr.* **1925**, *51* (44), 1809–1813.
- (16) Nissle, A. Die Antagonistische Behandlung Chronischer Darmstörungen Mit Colibakterien. *Med. Klin* **1918**, *2*, 29–33.
- (17) Sonnenborn, U.; Schulze, J. The Non-Pathogenic *Escherichia Coli* Strain *Nissle 1917*—Features of a Versatile Probiotic. *Microb. Ecol. Health Dis.* **2009**, *21* (3–4), 122–158.
- (18) Torres, J.; Bonovas, S.; Doherty, G.; Kucharzik, T.; Gisbert, J. P.; Raine, T.; Adamina, M.; Armuzzi, A.; Bachmann, O.; Bager, P.; Biancone, L.; Bokemeyer, B.; Bossuyt, P.; Burisch, J.; Collins, P.; El-Hussuna, A.; Ellul, P.; Frei-Lanter, C.; Furfaro, F.; Gingert, C.; Gionchetti, P.; Gomollon, F.; González-Lorenzo, M.; Gordon, H.; Hlavaty, T.; Juillerat, P.; Katsanos, K.; Kopylov, U.; Krustins, E.; Lytras, T.; Maaser, C.; Magro, F.; Kenneth Marshall, J.; Myrelid, P.; Pellino, G.; Rosa, I.; Sabino, J.; Savarino, E.; Spinelli, A.; Stassen, L.; Uzzan, M.; Vavricka, S.; Verstockt, B.; Warusavitarne, J.; Zmora, O.; Fiorino, G. ECCO Guidelines on Therapeutics in Crohn's Disease: Medical Treatment. *J. Crohns Colitis* **2020**, *14* (1), 4–22.
- (19) Raine, T.; Bonovas, S.; Burisch, J.; Kucharzik, T.; Adamina, M.; Annese, V.; Bachmann, O.; Bettenworth, D.; Chaparro, M.; Czuber-Dochan, W.; Eder, P.; Ellul, P.; Fidalgo, C.; Fiorino, G.; Gionchetti, P.; Gisbert, J. P.; Gordon, H.; Hedin, C.; Holubar, S.; Iacucci, M.; Karmiris, K.; Katsanos, K.; Kopylov, U.; Lakatos, P. L.; Lytras, T.; Lyutakov, I.; Noor, N.; Pellino, G.; Piovani, D.; Savarino, E.; Selvaggi, F.; Verstockt, B.; Spinelli, A.; Panis, Y.; Doherty, G. ECCO Guidelines on Therapeutics in Ulcerative Colitis: Medical Treatment. *J. Crohns Colitis* **2022**, *16* (1), 2–17.
- (20) Gordon, H.; Biancone, L.; Fiorino, G.; Katsanos, K. H.; Kopylov, U.; Al Sulais, E.; Axelrad, J. E.; Balendran, K.; Burisch, J.; De Ridder, L.; Derikx, L.; Ellul, P.; Greuter, T.; Iacucci, M.; Di Jiang, C.; Kapizioni, C.; Karmiris, K.; Kirchgessner, J.; Laharie, D.; Lobatón, T.; Molnár, T.; Noor, N. M.; Rao, R.; Saibeni, S.; Scharl, M.; Vavricka, S. R.; Raine, T. ECCO Guidelines on Inflammatory Bowel Disease and Malignancies. *J. Crohns Colitis* **2023**, *17* (6), 827–854.
- (21) Schultz, M. Clinical Use of *E. Coli Nissle 1917* in Inflammatory Bowel Disease. *Inflamm. Bowel Dis.* **2008**, *14* (7), 1012–1018.
- (22) Ukena, S. N.; Singh, A.; Dringenberg, U.; Engelhardt, R.; Seidler, U.; Hansen, W.; Bleich, A.; Bruder, D.; Franzke, A.; Rogler, G.; Suerbaum, S.; Buer, J.; Gunzer, F.; Westendorf, A. M. Probiotic *Escherichia Coli Nissle 1917* Inhibits Leaky Gut by Enhancing Mucosal Integrity. *PLoS One* **2007**, *2* (12), No. e1308.
- (23) Matthes, H.; Krummenerl, T.; Giensch, M.; Wolff, C.; Schulze, J. Clinical Trial: Probiotic Treatment of Acute Distal Ulcerative Colitis with Rectally Administered *Escherichia Coli Nissle 1917* (EcN). *BMC Complement. Altern. Med.* **2010**, *10* (1), 13.
- (24) Kruis, W. Maintaining Remission of Ulcerative Colitis with the Probiotic *Escherichia Coli Nissle 1917* Is as Effective as with Standard Mesalazine. *Gut* **2004**, *53* (11), 1617–1623.
- (25) Dong, Y.; Xu, T.; Xiao, G.; Hu, Z.; Chen, J. Opportunities and Challenges for Synthetic Biology in the Therapy of Inflammatory Bowel Disease. *Front. Bioeng. Biotechnol.* **2022**, *10*, 909591.
- (26) Lynch, J. P.; Goers, L.; Lesser, C. F. Emerging Strategies for Engineering *Escherichia Coli Nissle 1917*-Based Therapeutics. *Trends Pharmacol. Sci.* **2022**, *43* (9), 772–786.
- (27) Ba, F.; Zhang, Y.; Ji, X.; Liu, W.; Ling, S.; Li, J. Expanding the Toolbox of Probiotic *Escherichia Coli Nissle 1917* for Synthetic Biology. *Biotechnol. J.* **2024**, *19*, 2300327.
- (28) Kurtz, C. B.; Millet, Y. A.; Puurunen, M. K.; Perreault, M.; Charbonneau, M. R.; Isabella, V. M.; Kotula, J. W.; Antipov, E.; Dagon, Y.; Denney, W. S.; Wagner, D. A.; West, K. A.; Degar, A. J.; Brennan, A. M.; Miller, P. F. An Engineered *E. Coli Nissle* Improves Hyperammonemia and Survival in Mice and Shows Dose-Dependent Exposure in Healthy Humans. *Sci. Transl. Med.* **2019**, *11* (475), No. eaau7975.
- (29) Isabella, V. M.; Ha, B. N.; Castillo, M. J.; Lubkowicz, D. J.; Rowe, S. E.; Millet, Y. A.; Anderson, C. L.; Li, N.; Fisher, A. B.; West, K. A.; Reeder, P. J.; Momin, M. M.; Bergeron, C. G.; Guilmain, S. E.; Miller, P. F.; Kurtz, C. B.; Falb, D. Development of a Synthetic Live Bacterial Therapeutic for the Human Metabolic Disease Phenylketonuria. *Nat. Biotechnol.* **2018**, *36* (9), 857–864.
- (30) Praveschotinunt, P.; Duraj-Thatte, A. M.; Gelfat, I.; Bahl, F.; Chou, D. B.; Joshi, N. S. Engineered *E. coli Nissle 1917* for the delivery of matrix-tethered therapeutic domains to the gut. *Nat. Commun.* **2019**, *10* (1), 5580.
- (31) Gelfat, I.; Aqeel, Y.; Tremblay, J. M.; Jaskiewicz, J. J.; Shrestha, A.; Lee, J. N.; Hu, S.; Qian, X.; Magoun, L.; Sheoran, A.; Bedenice, D.; Giem, C.; Manjula-Basavanna, A.; Pulsifer, A. R.; Tu, H. X.; Li, X.; Minus, M. L.; Osburne, M. S.; Tzipori, S.; Shoemaker, C. B.; Leong, J. M.; Joshi, N. S. Single Domain Antibodies against Enteric Pathogen Virulence Factors Are Active as Curli Fiber Fusions on Probiotic *E. Coli Nissle 1917*. *PLoS Pathog.* **2022**, *18* (9), No. e1010713.
- (32) Zou, Z. P.; Du, Y.; Fang, T. T.; Zhou, Y.; Ye, B. C. Biomarker-Responsive Engineered Probiotic Diagnoses, Records, and Ameliorates Inflammatory Bowel Disease in Mice. *Cell Host Microbe* **2023**, *31* (2), 199–212.e5.
- (33) Lynch, J. P.; González-Prieto, C.; Reeves, A. Z.; Bae, S.; Powale, U.; Godbole, N. P.; Tremblay, J. M.; Schmidt, F. I.; Ploegh, H. L.; Kansra, V.; Glickman, J. N.; Leong, J. M.; Shoemaker, C. B.; Garrett, W. S.; Lesser, C. F. Engineered *Escherichia Coli* for the in Situ Secretion of Therapeutic Nanobodies in the Gut. *Cell Host Microbe* **2023**, *31* (4), 634–649.e8.
- (34) Liu, Y.; Zhu, Z.; Jiang, L. Programming Therapeutic Probiotics by Self-Tunable Sense-and-Respond Genetic Circuits. *Trends Microbiol.* **2023**, *31* (11), 1099–1101.
- (35) Soufli, I.; Toumi, R.; Rafa, H.; Touil-Boukoffa, C. Overview of Cytokines and Nitric Oxide Involvement in Immuno-Pathogenesis of Inflammatory Bowel Diseases. *World J. Gastrointest. Pharmacol. Ther.* **2016**, *7* (3), 353.
- (36) Avdagić, N.; Zaćiragić, A.; Babić, N.; Hukić, M.; Šeremet, M.; Lepara, O.; Nakaš-İćindić, E. Nitric Oxide as a Potential Biomarker in Inflammatory Bowel Disease. *Bosn. J. Basic Med. Sci.* **2013**, *13* (1), 5.
- (37) Schairer, D. O.; Chouake, J. S.; Nosanchuk, J. D.; Friedman, A. J. The Potential of Nitric Oxide Releasing Therapies as Antimicrobial Agents. *Virulence* **2012**, *3* (3), 271–279.
- (38) Chen, X. J.; Wang, B.; Thompson, I. P.; Huang, W. E. Rational Design and Characterization of Nitric Oxide Biosensors in *E. Coli Nissle 1917* and Mini SimCells. *ACS Synth. Biol.* **2021**, *10* (10), 2566–2578.
- (39) Muyldermans, S. Nanobodies: Natural Single-Domain Antibodies. *Annu. Rev. Biochem.* **2013**, *82*, 775–797.
- (40) Hamers-Casterman, C.; Atarhouch, T.; Muyldermans, S.; Robinson, G.; Hammers, C.; Songa, E. B.; Bendahman, N.; Hammers, R. Naturally Occurring Antibodies Devoid of Light Chains. *Nature* **1993**, *363* (6428), 446–448.

- (41) Vincke, C.; Loris, R.; Saerens, D.; Martinez-Rodriguez, S.; Muyldermans, S.; Conrath, K. General Strategy to Humanize a Camelid Single-Domain Antibody and Identification of a Universal Humanized Nanobody Scaffold. *J. Biol. Chem.* **2009**, *284* (5), 3273–3284.
- (42) Silence, K.; Lauwereys, M.; De Haard, H. Single Domain Antibodies Directed against Tumour Necrosis Factor-Alpha and Uses Therefor. U.S. Patent 20,090,022,721 A1, 2003.
- (43) Dalbey, R. E.; Kuhn, A. Protein Traffic in Gram-Negative Bacteria - How Exported and Secreted Proteins Find Their Way. *FEMS Microbiol. Rev.* **2012**, *36* (6), 1023–1045.
- (44) Holland, I. B.; Kenny, B.; Blight, M. Haemolysin Secretion from *E. Coli*. *Biochimie* **1990**, *72* (2–3), 131–141.
- (45) Blight, M. A.; Chervaux, C.; Holland, I. B. Protein Secretion Pathways in *Escherichia Coli*. *Curr. Opin. Biotechnol.* **1994**, *5* (5), 468–474.
- (46) Green, E. R.; Meccas, J. Bacterial Secretion Systems: An Overview. *Virulence mechanisms of bacterial pathogens* **2016**, 213–239.
- (47) Fraile, S.; Muñoz, A.; De Lorenzo, V.; Fernández, L. A. Secretion of Proteins with Dimerization Capacity by the Haemolysin Type I Transport System of *Escherichia Coli*. *Mol. Microbiol.* **2004**, *53* (4), 1109–1121.
- (48) Ruano-Gallego, D.; Fraile, S.; Gutierrez, C.; Fernández, L. A. Screening and Purification of Nanobodies from *E. Coli* Culture Supernatants Using the Hemolysin Secretion System. *Microb. Cell Fact.* **2019**, *18* (1), 47.
- (49) Hutchings, M. I.; Mandhana, N.; Spiro, S. The NorR Protein of *Escherichia Coli* Activates Expression of the Flavorubredoxin Gene *NorV* in Response to Reactive Nitrogen Species. *J. Bacteriol.* **2002**, *184* (16), 4640–4643.
- (50) Gardner, A. M.; Gessner, C. R.; Gardner, P. R. Regulation of the Nitric Oxide Reduction Operon (NorRVW) in *Escherichia Coli*. *J. Biol. Chem.* **2003**, *278* (12), 10081–10086.
- (51) D'Autréaux, B.; Tucker, N. P.; Dixon, R.; Spiro, S. A Non-Haem Iron Centre in the Transcription Factor NorR Senses Nitric Oxide. *Nature* **2005**, *437* (7059), 769–772.
- (52) Tucker, N. P.; D'Autréaux, B.; Spiro, S.; Dixon, R. Mechanism of Transcriptional Regulation by the *Escherichia Coli* Nitric Oxide Sensor NorR. *Biochem. Soc. Trans.* **2006**, *34* (1), 191–194.
- (53) Pédelacq, J. D.; Cabantous, S.; Tran, T.; Terwilliger, T. C.; Waldo, G. S. Engineering and Characterization of a Superfolder Green Fluorescent Protein. *Nat. Biotechnol.* **2006**, *24* (1), 79–88.
- (54) Mancinelli, R. L.; McKay, C. P. Effects of Nitric Oxide and Nitrogen Dioxide on Bacterial Growth. *Appl. Environ. Microbiol.* **1983**, *46* (1), 198–202.
- (55) Korostelev, A. A. The Structural Dynamics of Translation. *Annu. Rev. Biochem.* **2022**, *91* (1), 245–267.
- (56) Gingold, H.; Pilpel, Y. Determinants of Translation Efficiency and Accuracy. *Mol. Syst. Biol.* **2011**, *7*, 481.
- (57) Unoson, C.; Wagner, E. G. H. Dealing with Stable Structures at Ribosome Binding Sites: Bacterial Translation and Ribosome Standby. *RNA Biol.* **2007**, *4* (3), 113–117.
- (58) Zimmermann, I.; Eglöf, P.; Hutter, C. A.; Arnold, F. M.; Stohler, P.; Bocquet, N.; Hug, M. N.; Huber, S.; Siegrist, M.; Hetemann, L.; Gera, J.; Gmür, S.; Spies, P.; Gyöax, D.; Geertsma, E. R.; Dawson, R. J.; Seeger, M. A. Synthetic Single Domain Antibodies for the Conformational Trapping of Membrane Proteins. *Elife* **2018**, *7*, No. e34317.
- (59) Lee, S. H.; Kwon, J.; Cho, M.-L. Immunological Pathogenesis of Inflammatory Bowel Disease. *Intest Res.* **2018**, *16* (1), 26.
- (60) Scheinfeld, N. Adalimumab (HUMIRA): A Review. *J. Drugs Dermatol.* **2003**, *2* (4), 375.
- (61) Schöneberg, J.; Ullrich, A.; Noé, F. Simulation Tools for Particle-Based Reaction-Diffusion Dynamics in Continuous Space. *BMC Biophys.* **2014**, *7* (1), 11.
- (62) Andrews, S. S.; Bray, D. Stochastic Simulation of Chemical Reactions with Spatial Resolution and Single Molecule Detail. *Phys. Biol.* **2004**, *1* (3), 137–151.
- (63) Chew, W.-X.; Kaizu, K.; Watabe, M.; Muniandy, S. V.; Takahashi, K.; Arjunan, S. N. V. Surface Reaction-Diffusion Kinetics on Lattice at the Microscopic Scale. *Phys. Rev. E* **2019**, *99* (4), 042411.
- (64) Kerr, R. A.; Bartol, T. M.; Kaminsky, B.; Dittrich, M.; Chang, J.-C. J.; Baden, S. B.; Sejnowski, T. J.; Stiles, J. R. Fast Monte Carlo Simulation Methods for Biological Reaction-Diffusion Systems in Solution and on Surfaces. *SIAM J. Sci. Comput.* **2008**, *30* (6), 3126–3149.
- (65) Radhakrishnan, K.; Halász, Á.; McCabe, M. M.; Edwards, J. S.; Wilson, B. S. Mathematical Simulation of Membrane Protein Clustering for Efficient Signal Transduction. *Ann. Biomed. Eng.* **2012**, *40* (11), 2307–2318.
- (66) Lacruz-Guzmán, D.; Torres-Moreno, D.; Pedrero, F.; Romero-Cara, P.; García-Tercero, I.; Trujillo-Santos, J.; Conesa-Zamora, P. Influence of polymorphisms and TNF and IL1 $\beta$  serum concentration on the infliximab response in Crohn's disease and ulcerative colitis. *Eur. J. Clin. Pharmacol.* **2013**, *69* (3), 431–438.
- (67) Iwaki, T.; Hara, K.; Umemura, K. Nanobody Production Can Be Simplified by Direct Secretion from *Escherichia Coli*. *Protein Expression Purif.* **2020**, *170*, 105607.
- (68) Sender, R.; Fuchs, S.; Milo, R. Revised Estimates for the Number of Human and Bacteria Cells in the Body. *PLoS Biol.* **2016**, *14* (8), No. e1002533.
- (69) McCallum, G.; Tropini, C. The Gut Microbiota and Its Biogeography. *Nat. Rev. Microbiol.* **2024**, *22*, 105–118.
- (70) Stein, R. R.; Tanoue, T.; Szabady, R. L.; Bhattarai, S. K.; Olle, B.; Norman, J. M.; Suda, W.; Oshima, K.; Hattori, M.; Gerber, G. K.; Sander, C.; Honda, K.; Bucci, V. Computer-Guided Design of Optimal Microbial Consortia for Immune System Modulation. *Elife* **2018**, *7*, No. e30916.
- (71) Aogo, R. A.; Tanaka, M. M.; Penington, C. J. Spatial Dynamics of Inflammation-Causing and Commensal Bacteria in the Gastrointestinal Tract. *J. Theor. Biol.* **2022**, *548*, 111194.
- (72) Labarthe, S.; Polizzi, B.; Phan, T.; Goudon, T.; Ribot, M.; Laroche, B. A Mathematical Model to Investigate the Key Drivers of the Biogeography of the Colon Microbiota. *J. Theor. Biol.* **2019**, *462*, 552–581.
- (73) Arciero, J. C.; Ermentrout, G. B.; Upperman, J. S.; Vodovotz, Y.; Rubin, J. E. Using a Mathematical Model to Analyze the Role of Probiotics and Inflammation in Necrotizing Enterocolitis. *PLoS One* **2010**, *5* (4), No. e10066.
- (74) Maria Spagnuolo, A.; DiRita, V.; Kirschner, D. A Model for *Vibrio Cholerae* Colonization of the Human Intestine. *J. Theor. Biol.* **2011**, *289*, 247–258.
- (75) Thomas, D. D.; Liu, X.; Kantrow, S. P.; Lancaster, J. R. The Biological Lifetime of Nitric Oxide: Implications for the Perivascular Dynamics of NO and O<sub>2</sub>. *Proc. Natl. Acad. Sci. U.S.A.* **2001**, *98* (1), 355–360.
- (76) Malinski, T.; Taha, Z.; Grunfeld, S.; Patton, S.; Kapturczak, M.; Tomboulian, P. Diffusion of Nitric Oxide in the Aorta Wall Monitored in Situ by Porphyrinic Microsensors. *Biochem. Biophys. Res. Commun.* **1993**, *193* (3), 1076–1082.
- (77) Triassi, A. J.; Fields, B. D.; Monahan, C. E.; Means, J. M.; Park, Y.; Doosthosseini, H.; Padmakumar, J. P.; Isabella, V. M.; Voigt, C. A. Redesign of an *Escherichia Coli* Nissle Treatment for Phenylketonuria Using Insulated Genomic Landing Pads and Genetic Circuits to Reduce Burden. *Cell Syst.* **2023**, *14* (6), 512–524.e12.
- (78) Wu, G.; Yan, Q.; Jones, J. A.; Tang, Y. J.; Fong, S. S.; Koffas, M. A. G. Metabolic Burden: Cornerstones in Synthetic Biology and Metabolic Engineering Applications. *Trends Biotechnol.* **2016**, *34* (8), 652–664.
- (79) Borkowski, O.; Ceroni, F.; Stan, G. B.; Ellis, T. Overloaded and Stressed: Whole-Cell Considerations for Bacterial Synthetic Biology. *Curr. Opin. Microbiol.* **2016**, *33*, 123–130.
- (80) Elowitz, M. B.; Levine, A. J.; Siggia, E. D.; Swain, P. S. Stochastic Gene Expression in a Single Cell. *Science* **2002**, *297* (5584), 1183–1186.

- (81) Bandiera, L.; Furini, S.; Giordano, E. Phenotypic Variability in Synthetic Biology Applications: Dealing with Noise in Microbial Gene Expression. *Front. Microbiol.* **2016**, *7*, 479.
- (82) Tropini, C.; Earle, K. A.; Huang, K. C.; Sonnenburg, J. L. The Gut Microbiome: Connecting Spatial Organization to Function. *Cell Host Microbe* **2017**, *21* (4), 433–442.
- (83) Del Vecchio, D.; Qian, Y.; Murray, R. M.; Sontag, E. D. Future Systems and Control Research in Synthetic Biology. *Annu. Rev. Control* **2018**, *45*, 5–17.
- (84) Choudhary, R.; Mahadevan, R. Toward a Systematic Design of Smart Probiotics. *Curr. Opin. Biotechnol.* **2020**, *64*, 199–209.
- (85) Rohllhill, J.; Sandoval, N. R.; Papoutsakis, E. T. Sort-Seq Approach to Engineering a Formaldehyde-Inducible Promoter for Dynamically Regulated Escherichia Coli Growth on Methanol. *ACS Synth. Biol.* **2017**, *6* (8), 1584–1595.
- (86) Cobb, R. E.; Sun, N.; Zhao, H. Directed Evolution as a Powerful Synthetic Biology Tool. *Methods* **2013**, *60* (1), 81–90.
- (87) Westmann, C. A.; Guazzaroni, M.-E.; Silva-Rocha, R. Engineering Complexity in Bacterial Regulatory Circuits for Biotechnological Applications. *mSystems* **2018**, *3* (2), 001511-17.
- (88) Antunes Westmann, C.; Goldbach, L.; Wagner, A. The Highly Rugged yet Navigable Regulatory Landscape of the Bacterial Transcription Factor TetR. *bioRxiv* **2023**, DOI: [10.1101/2023.08.25.554764](https://doi.org/10.1101/2023.08.25.554764).
- (89) Moon, T. S. Probiotic and Microbiota Engineering for Practical Applications. *Curr. Opin. Food Sci.* **2024**, *56*, 101130.
- (90) Barra, M.; Danino, T.; Garrido, D. Engineered Probiotics for Detection and Treatment of Inflammatory Intestinal Diseases. *Front. Bioeng. Biotechnol.* **2020**, *8*, 521594.
- (91) Brooks, S. M.; Alper, H. S. Applications, Challenges, and Needs for Employing Synthetic Biology beyond the Lab. *Nat. Commun.* **2021**, *12* (1), 1390.
- (92) Kumar, S.; Hasty, J. Stability, Robustness, and Containment: Preparing Synthetic Biology for Real-World Deployment. *Curr. Opin. Biotechnol.* **2023**, *79*, 102880.
- (93) Ingram, D.; Stan, G.-B. Modelling Genetic Stability in Engineered Cell Populations. *Nat. Commun.* **2023**, *14* (1), 3471.
- (94) Olier, M.; Marcq, I.; Salvador-Cartier, C.; Secher, T.; Dobrindt, U.; Boury, M.; Bacquié, V.; Penary, M.; Gaultier, E.; Nougayrède, J. P.; Fioramonti, J.; Oswald, E. Genotoxicity of Escherichia Coli Nissle 1917 Strain Cannot Be Dissociated from Its Probiotic Activity. *Gut Microbes* **2012**, *3* (6), 501–509.
- (95) Nougayrède, J. P.; Chagneau, C. V.; Motta, J.-P.; Bossuet-Greif, N.; Belloy, M.; Taieb, F.; Gratadoux, J.-J.; Thomas, M.; Langella, P.; Oswald, E. A Toxic Friend: Genotoxic and Mutagenic Activity of the Probiotic Strain Escherichia Coli Nissle 1917. *mSphere* **2021**, *6* (4), No. e00624-21.
- (96) Tramontano, M.; Andrejev, S.; Pruteanu, M.; Klünemann, M.; Kuhn, M.; Galardini, M.; Jouhten, P.; Zelezniak, A.; Zeller, G.; Bork, P.; Typas, A.; Patil, K. R. Nutritional Preferences of Human Gut Bacteria Reveal Their Metabolic Idiosyncrasies. *Nat. Microbio.* **2018**, *3* (4), 514–522.
- (97) Heinken, A.; Acharya, G.; Ravcheev, D. A.; Hertel, J.; Nyga, M.; Okpala, O. E.; Hogan, M.; Magnúsdóttir, S.; Martinelli, F.; Preciat, G.; et al. AGORA2: Large Scale Reconstruction of the Microbiome Highlights Wide-Spread Drug-Metabolising Capacities. *bioRxiv* **2020**, DOI: [10.1101/2020.11.09.375451](https://doi.org/10.1101/2020.11.09.375451).
- (98) van 't Hof, M.; Mohite, O. S.; Monk, J. M.; Weber, T.; Palsson, B. O.; Sommer, M. O. A. High-Quality Genome-Scale Metabolic Network Reconstruction of Probiotic Bacterium Escherichia Coli Nissle 1917. *BMC Bioinf.* **2022**, *23* (1), 566.
- (99) Nørholm, M. H. H. Meta Synthetic Biology: Controlling the Evolution of Engineered Living Systems. *Microb. Biotechnol.* **2018**, *12*, 35–37.
- (100) Mays, Z. J. S.; Chappell, T. C.; Nair, N. U. Quantifying and Engineering Mucus Adhesion of Probiotics. *ACS Synth. Biol.* **2020**, *9* (2), 356–367.
- (101) Kan, A.; Gelfat, I.; Emani, S.; Praveschotinunt, P.; Joshi, N. S. Plasmid Vectors for *in Vivo* Selection-Free Use with the Probiotic E. Coli Nissle 1917. *ACS Synth. Biol.* **2021**, *10* (1), 94–106.
- (102) Sundaram, L. S.; Ajioka, J. W.; Molloy, J. C. Synthetic Biology Regulation in Europe: Containment, Release and Beyond. *Synth. Biol.* **2023**, *8* (1), ysad009.
- (103) Donati, S.; Barbier, I.; García-Soriano, D. A.; Grasso, S.; Handal-Marquez, P.; Malci, K.; Marlow, L.; Westmann, C.; Amara, A. Synthetic Biology in Europe: Current Community Landscape and Future Perspectives. *Biotechnol. Notes* **2022**, *3*, 54–61.
- (104) Karabin, J.; Mansfield, I.; Frow, E. K. Exploring Presentations of Sustainability by US Synthetic Biology Companies. *PLoS One* **2021**, *16* (9), No. e0257327.
- (105) Voigt, C. A. Synthetic Biology 2020–2030: Six Commercially-Available Products That Are Changing Our World. *Nat. Commun.* **2020**, *11* (1), 6379.